修士論文

A novel nanomesh humidity sensor for continuous skin moisture monitoring (連続的な皮膚水分モニタリングのためのナノメッシュ湿度センサー)

令和 4 年 7 月 25 日 提出

指導教員：染谷隆夫　　教授

東京大学大学院工学系研究科

電気系工学専攻 37－205023

王文清

Contents

Abstract

The continuous monitoring of human physiological signals using on-skin wearable sensors is highly demanded for improving of quality of life. The development of physiological sensors that can be conformably attached to human skin for the long term is the central issue of wearable electronics.

Among the biophysical signals, the humidity value is one of the important parameters that are highly related to human health, reflecting the skin barrier functions, and the skin thermoregulation functions. The skin humidity level also has a relationship with skin diseases such as atopic dermatitis or hair loss. It is necessary to develop a skin-attachable humidity sensor that does not influence the basic operation of the skin functions and does not change the measurement results by sweating accumulation.

The previous works focused on the development of flexible humidity sensors and highly sensitive humidity sensors have greatly advanced the solving of this problem. However, the development of gas-permeable humidity sensors together with high sensitivity is still not achieved. The difficulty of integrating porous electrodes and porous sensitive materials is the main reason limiting the development of the sensor.

In this work, we firstly realized a humidity sensor with gas-permeability, high sensitivity, and flexibility together. The unique nanomesh structure is the main reason to achieve such a property. The porous structure is the cause of the flexibility and gas-permeability, and also increases the surface area that can contribute to a high sensitivity.

The sensor has a high sensitivity of 640,000% in the 40–100% relative humidity range. At the same time, it has a high gas permeability which is same to the performance of an open environment. The gas permeability suppresses skin inflammation, endows natural evaporation of sweat, and brings an identical condition to bare skin. To evaluate the utility of the nanomesh sensor, on-skin humidity measurements are performed, and the humidity change due to sweating after exercise is recorded.

All details of the development of the gas-permeable nanomesh humidity sensor are discussed in this thesis, including the fabrication process, sensor characterization, circuit model, and the application as on-skin measurement.

1. Introduction

1.1 Background

Nowadays, the demand for high-quality healthcare and improving life quality is rapidly growing[1, 2]. Due to the aging society development, the need for remote health monitoring, unmanned monitoring, and at-home healthcare is increasing to attract attention [3-5]. By comparing with the bulky equipment and specialized doctors and nurses at the hospital, how to realize the monitoring and diagnosis of health status at home is a great challenge for realizing a high-quality healthcare system.

Recently, commercialized wearable devices in the form of small, rigid blocks of wireless electronic/sensing components which were usually coupled with the human wrist were growing popular, such as Apple Watch[6]. The wearable electronics systems which integrated physiological signal sensors, analog front circuits, signal processing circuits, wireless communication modules, and power sources together become a promising method for the solution of healthcare in the future generation[7-12].

However, the current electronic systems rely on silicon integrated circuit chips. The biology tissues are soft and able to be bent, which has a large mechanical mismatch between silicon-based plate circuits[13]. Instead, the use of inherently soft electronic materials that have a low Young's modulus to directly contact biological tissues can minimize adverse reactions, owing to the improved mechanical compliance. The wearable soft electronics with the ability to be operated in a long term can contribute to the realization of individualized healthcare and early detection of chronic diseases.

Skin is the largest organ of humans. The health monitoring by the different kinds of on-skin physiological sensors, such as bioelectrical signals, bio-physical signals, and bio-chemical signals helps users to know the health status of the human body in time. To realize the target, skin electronics are developed with the innovation of structures, materials, sensors, and developed new functions. Figure 1.1 summarized some of the recent development in the on-skin electronic systems.

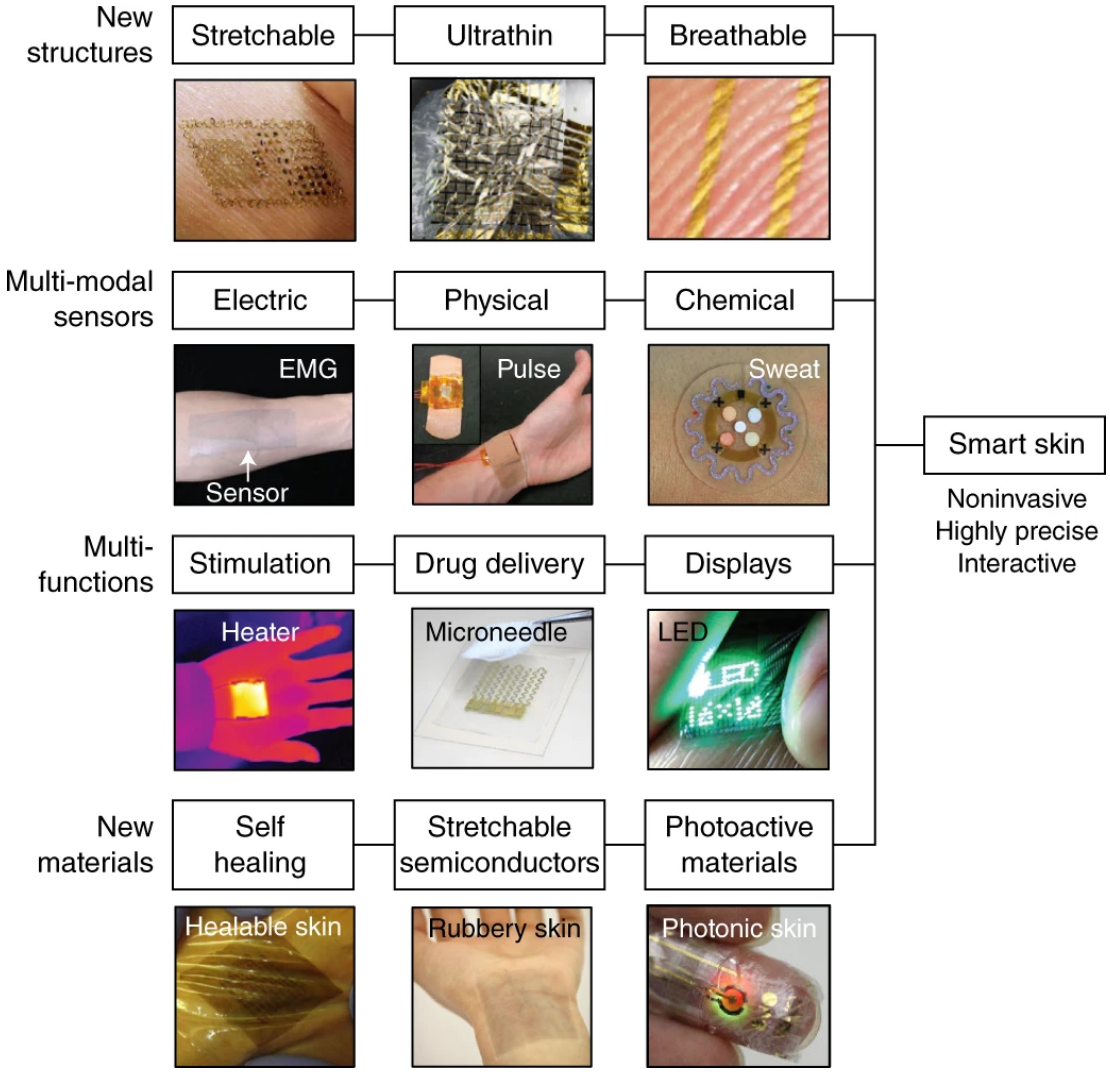

Figure 1.1 The recent development of on-skin electronics, copied from reference[2].

The development of thin, soft, stretchable, breathable materials and structures is now endowing more and more properties to the on-skin systems. The decrease of the thickness helps the intimate contact with human skin, decreases the skin contact impedance, increases the signal qualities, and allows the free movement and function of the human body and skin[13]. The other functions such as intrinsic stretchability[14, 15], self-healing[16], drug delivery[17], and gas-permeability[18] are added to the devices to realize more functions.

Biophysical signals are one kind of physiological signal that measures the basic physical properties related to the human body, such as the physical motions, temperature, and humidity, skin properties, skeletal muscles, pressure, and strains.

Figure 1.2 summarized the commonly seen biophysical targets and their sensing mechanisms.

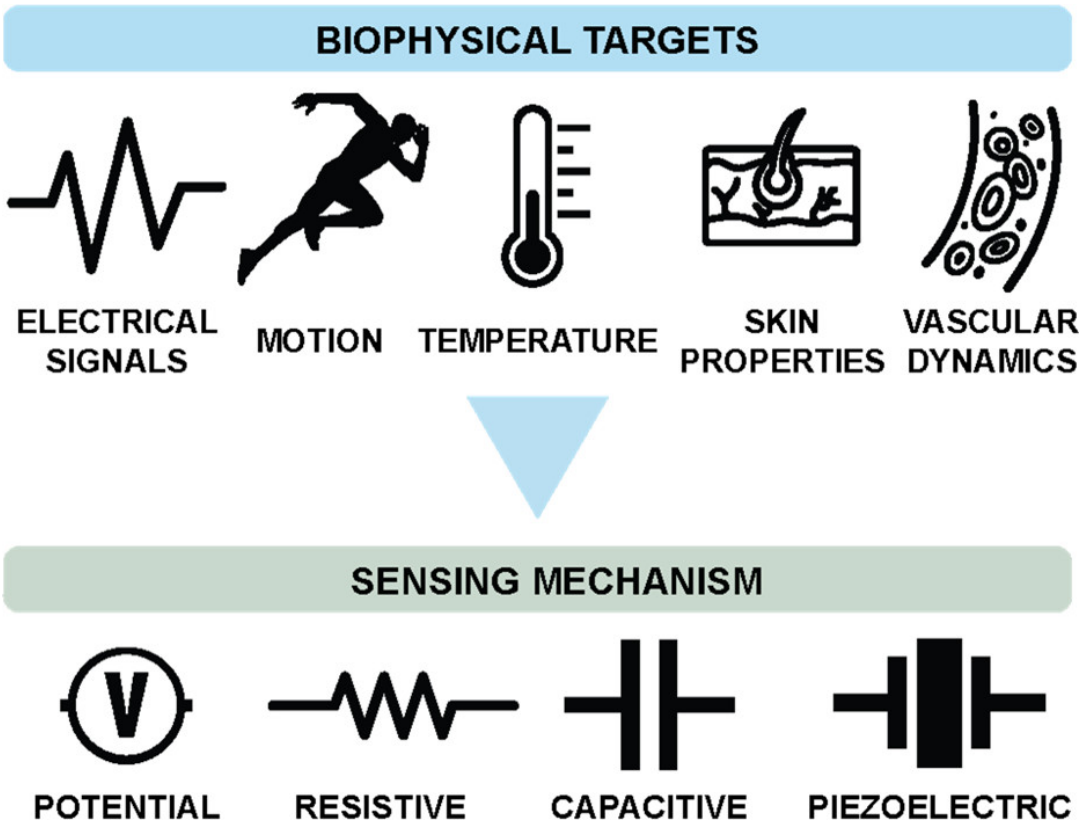

Figure 1.2 The biophysical signals and the related sensing mechanisms, copied from the reference[3].

As one of the most important biophysical signals, bioelectrical signals provide effective information about the human body. Bioelectrical signals are signals that are recorded by bio-interfaced electrodes for biopotential signals such as the electrocardiogram (ECG), Electromyography (EMG), and electroencephalogram (EEG) signals.

The electrical impedance is one of the most important properties to quantify the electrode-skin interface. A stable, compact, and reliable interface result in a stable and low impedance. A high interface impedance leads to a decrease in the efficacy of common mode noise rejection due to the amplified differences between electrodes. Also, the mechanical interfaces help to increase the adhesion force between the electrode and skin, which leads to a larger bonding force and a lower motion-artifact noise. Soft electronics which realize conformable and low impedance attachment are the

mainstream of research.

Another important category of biosensors is biochemical sensors. Apart from physical signals and electrical signals, the chemical contents in the multiple biofluids provided a new window for knowing the complete scene of the human health status. The conventional biochemical measurements require expensive analytical instruments at hospitals and require invasively sampling of biofluids like human blood. The wearable biochemical sensors usually have a stable interface with skin and utilize non-invasive methods for measurement. The receptor layer combines with the target chemicals and then generates a signal to the transducer layer, the transducer layer will transform the signal into electrical or optical signals that can be easily read out by supplementary circuits. Figure 1.3 summarized the typical biochemical sensors and their operation principles.

Figure 1.3 The typical biochemical targets, receptors, and sensing methods, copied from the reference[3].

1.2 Human humidity

Humidity is one of the important physical parameters that describe the water molecule contents in the air. Water molecules are existing everywhere in air and range from nearly 0% to more than 4% of the mass of air[19]. Humidity value can be useful in many fields, such as industry[20], biomedical monitoring[21-27], weather forecasting[28], agriculture products[29, 30], high energy physics[31]. Extremely high or low humidity values will cause lives dead or ill, and cause machines and devices damage. A suitable range of humidity values is essential for human and machine health. The measurement and control of humidity are needed for the automation of many applications. The humidity data can also contribute to the development of IoT and wearable systems. Figure 1.4 shows some of these applications of humidity value.

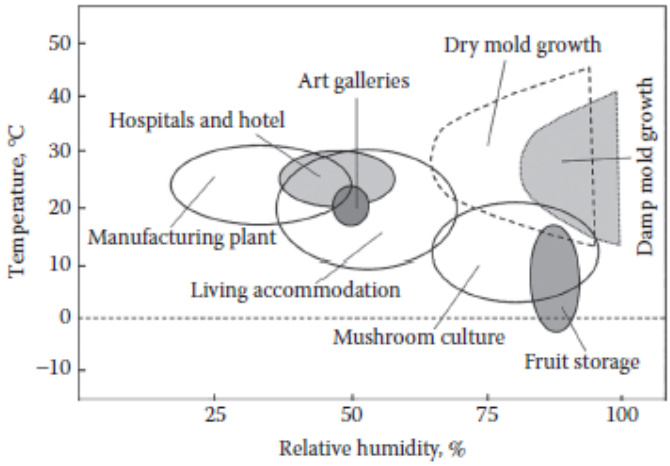

Figure 1.4 Optimal temperature and relative humidity for daily applications, copied from the reference[19].

Like temperature, humidity is also a physical environmental factor that influences human comfort and health. Previous works have shown that air humidity has a strong influence on people's comfort with air[32-34]. The human body is usually sensitive to the outside air atmosphere since it is most often exposed to the surrounding air environment.

The human perception of air to the relative humidity value and temperature were

concluded in the following Table 1.1, based on the reference[19]. The humidity change in the environment strongly influences the human body's reaction based on sweat secretion and evaporation. Figure 1.5 shows the comfortable zone of temperature and humidity for human living.

Table 1.1 Effect of temperature and humidity on human perception of air.

Table 6.1. Influence of temperature and humidity on human

RH at 32 ℃	**Dew point**	**Human perception**
≥73%	Over 26℃	Severely high. Even deadly for asthmarelated illnesses
62%-72%	24℃-26℃	Extremely uncomfortable, fairly oppressive
52%-61%	21℃-24℃	Very humid, quite uncomfortable
44%-51%	18℃-21℃	Somewhat uncomfortable for most people at upper edge
37%-43%	16℃-18℃	OK for most, but all perceive the humidity at upper edge
31%-36%	13℃-16℃	Comfortable
26%-30%	10℃-12℃	Very comfortable
≤25%	Under 10℃	A bit dry for some

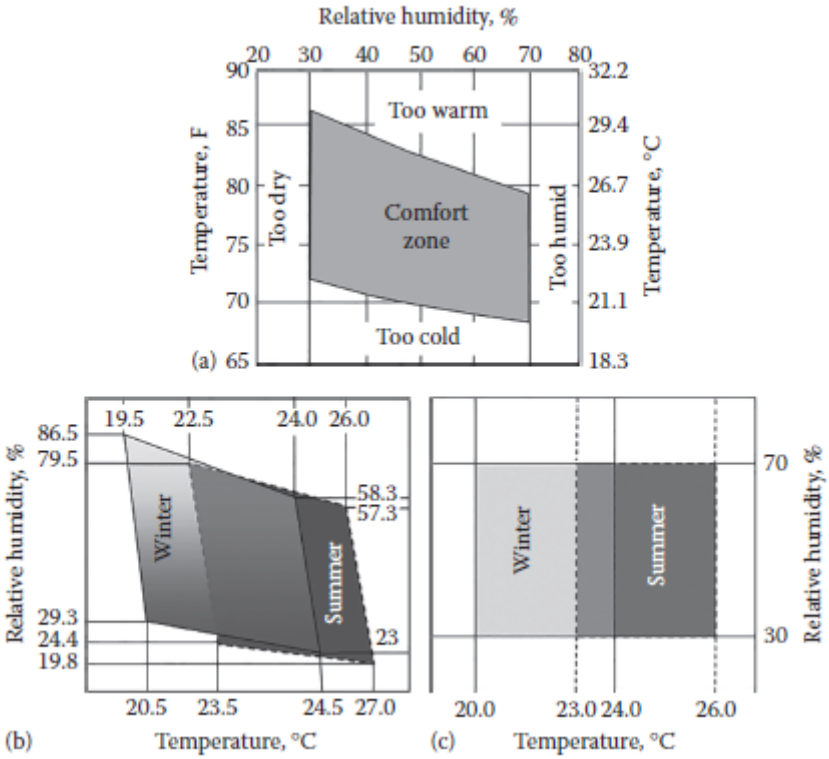

Figure 1.5 Chart illustrating zone for comfort living. Copied from reference[19]

If the air has a high temperature, the human body tries to use the evaporation of sweat on skin to cool down the core temperature of the body. The rate of the thermoregulation method is directly related to how fast the sweat is evaporating. In high moisture air, the evaporation rate will become lower. When the air becomes drier, the body starts to lose moisture, and a high Trans-Epidermal Water Loss (TEWL) will happen on the skin surface. This loss of water from the skin is always happening and is not immediately noticeable, but if the water content is restored in the body in time, there may cause serious complications related to dehydration. At the same time, the moisture that air can contain depends on the temperature of the air, the high temperature increases the absolute humidity in the air. Therefore, a particularly dangerous situation is the combination of high humidity with high temperatures. The reduction of evaporation rate can cause considerable discomfort or lead to a heat stroke, which may cause death[35].

On the other hand, if the excess heat can not be dissipated outside by TEWL, the human

body will be disturbed due to a high heat load, which is usually observed in diseases such as fever and hyperthyroidism[22].

The skin humidity level is also related to the skin diseases such as atopic dermatitis or hair loss. Previous works have pointed out that the 1-2 days of dry environment provokes epidermal proliferation, and reduction in skin hydration, a proinflammatory and a transient barrier deficit. The increased thickness of the SC layer and enhanced barrier function will form on the skin surface, which leads to a decrease in TEWL. The measured humidity value on the skin surface will also decrease. Therefore, the monitoring of skin humidity can reflect the health status of the skin. Figure 1.6 shows the influence of a dry environment on human skin health.

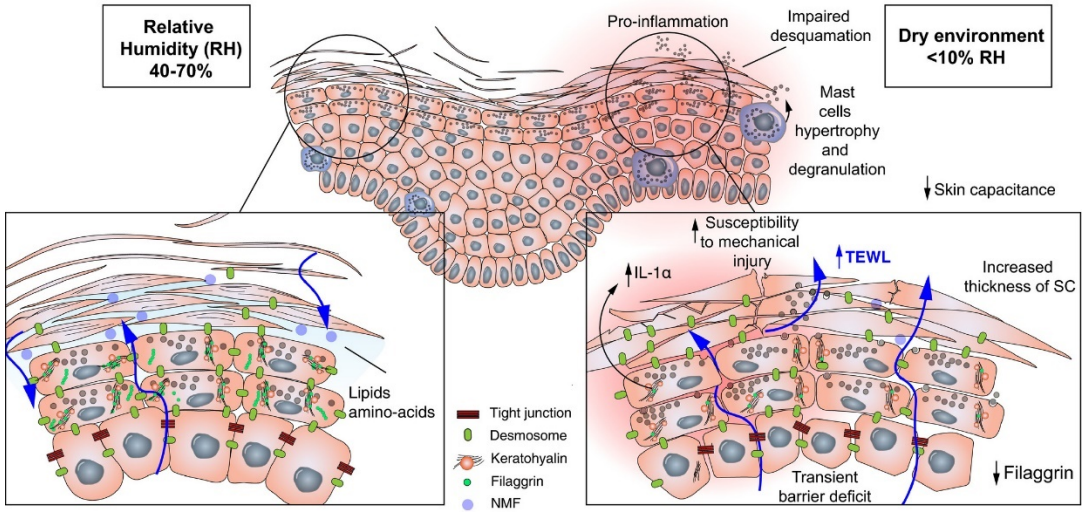

Figure 1.6 The influence of the dry environment (RH<10%) on skin barrier function and composition, copied from reference, copied from reference [36].

In order to know the health status of the skin for thermoregulation and barrier function, the continuous monitoring of skin temperature and skin humidity together is necessary. In this work, the nanomesh humidity sensor which exhibits similar gas and water vapor permeability is utilized for skin humidity detection, which avoids the accumulation of sweat on the skin surface, and allows the measurement result of the skin humidity to be not disturbed. At the same time, the gas-permeability avoids the cause of skin inflammation and hair loss[18].

1.3 Mechanism

1.3.1 Humidity units

Different kinds of methods can be used to show the water contents concentration in the air. The most commonly used units are relative humidity (RH), Dew/Frost point (D/F PT), and Parts Per Million (PPM). Relative humidity has two commonly used definitions[37]. One of the definitions is the actual water vapor dry mass ratio w to the equilibrium (also called saturation) mixing ratio w_s at the ambient temperature and pressure, which is regarded as a standard definition:

$$RH = \frac{w}{w_s} \times 100\% \quad (1)$$

Another definition is the ratio of the actual water vapor pressure p to the equilibrium vapor pressure over a plane of water p_s. (usually called saturation vapor pressure).

$$RH = \frac{p}{p_s} \times 100\% \quad (2)$$

The two definitions are related by $w = \varepsilon p(P-p)^{-1}$ and $w_s = \varepsilon p_s(P-p_s)^{-1}$. Where ε (0.622) is the ratio of the molecular weights of water and dry air. Usually, the ambient air pressure P is high enough compared with the water vapor pressure. So, the two definitions are approximately the same. The relative humidity is "relative" because the temperature will influence the water vapor pressure (mass), so it is dependent on temperature.

For the further precise measurement of humidity, Dew/Frost point is usually considered. The Dew point is the temperature (above 0℃) that the water vapor in the gas condenses to liquid water. Frost point is the temperature (below 0℃) that the water vapor condenses to ice. D/F point is an absolute value that is not influenced by temperature. The Dew/Frost point shows the exponential relationship with relative humidity and can present faint humidity changing.

Parts Per Million (PPM) is another commonly used definition. The PPM value shows

the volume fraction of water vapor in the air. PPM also shows an absolute measurement.

The three different humidity units are used under different applications. Figure 1.7 shows the humidity range of different methods.

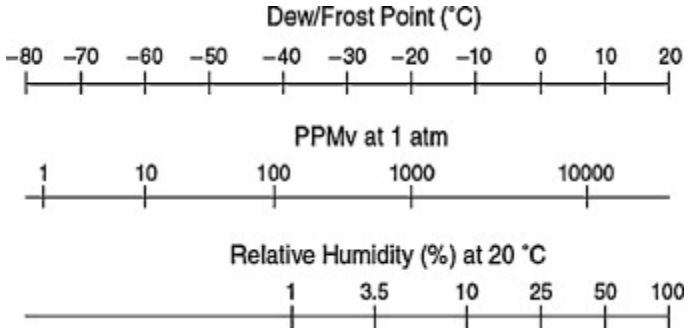

Figure 1.7 Relationship between Relative humidity (RH), Dew/Frost point (D/F PT), and Parts Per Million by volume fraction (PPMv).

1.3.2 Capillary effect

The mechanism of the nanomesh humidity sensor could be highly related to the capillary effect of the polymer. Water condensation of water vapor takes place within the porous structure of the polymer chains. The amount of the condensed polymer will be influenced by the pores size, pores distributions, and pores volume[38].

In a simplified situation, the pores of the polymers are considered cylindrical pores, then the pore radius at which capillary condensation starts to happen can be shown by the Kelvin equation[39].

$$r = \frac{2\gamma M}{\rho RT \ln \frac{p_S}{p}} \tag{3}$$

Where r, γ, and ρ are the pore radius at which capillary condensation is ready to happen, the surface tension, the molecular weight, and the density of the water, respectively. p is the water vapor pressure and ps is the water vapor pressure at saturation, p/ps approximately equals RH in the first approximation.

1.3.3 Electrical property change

Water absorption in the pore space of the nanomesh structure will lead to the electrical properties of the sensor change. Water has a high relative dielectric constant (which is more than 80) when compared to air (which is 1), and waster has high conductivity (10^{-6} S/cm ~ 10^{-5} S/cm) when compared to air (10^{-14}S/cm). The increase in the water concentration ratio in the hybrid structure leads to a change in the overall dielectric constant and the conductivity of the whole structure.

However, the water condensation and evaporation are asymmetric. The evaporation takes more energy than the condensation process, so usually, the humidity sensor will have a longer desorption time in the absorption time, and even causes hysteresis.

1.4 Previous works of wearable humidity sensor

1.4.1 Flexibility

In recent years, considerable efforts have been directed towards the realization of flexible humidity sensors as on-skin wearable electronics.

Stefano Borini et. al. developed an ultrafast graphene oxide humidity sensor[40]. Figure 1.8 shows the sensor characteristics. The sensor was fabricated on a PEN substrate (Teijin Dupont Films). Graphene oxide was deposited as humidity-sensitive materials and Ag was screen printed as electrodes. The ultrathin graphene film of 15 nm decreased the response time down to ~30 ms. The porous two-dimensional materials show characteristics such as sub-nanometer pore size, atomic thinness, and facile manufacturing processes.

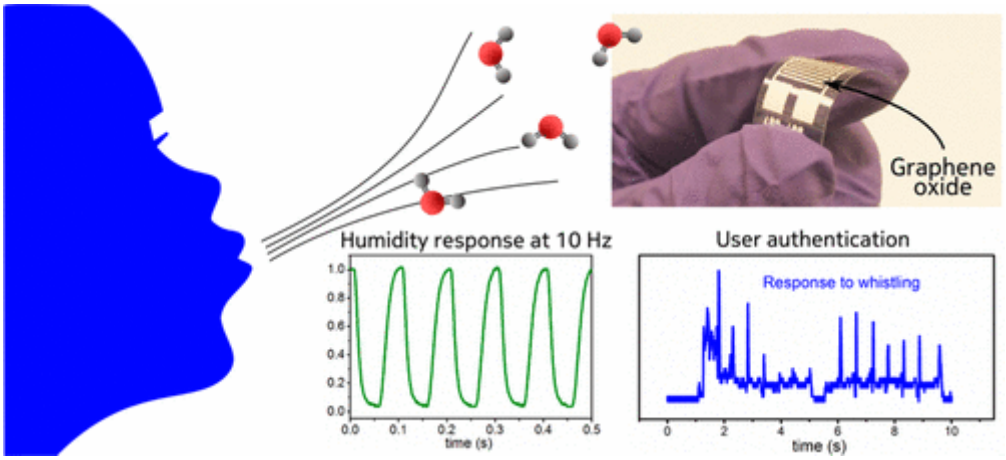

Figure 1.8 The basic characteristics of graphene oxide humidity sensor, copied from the reference[40].

Jin Wu et. al. developed a carbon nanocoil-based fast-response and flexible humidity sensor[41]. A flexible liquid crystal polymer was used for the fabrication of a substrate. The sensor shows a fast response of 1.9s and recovery of 1.5s, a broad detection range of 4-95%, linearity, repeatability, and stability. The hydrophobic effect of the LCP substrate and high purity of the CNCs give a ride to weak physical adsorption. The flexibility of bending and twisting is due to the helical structure of CNCs and the microporous structure of the LCP substrate. Figure 1.9 shows the basic properties of the carbon nanocoil sensor.

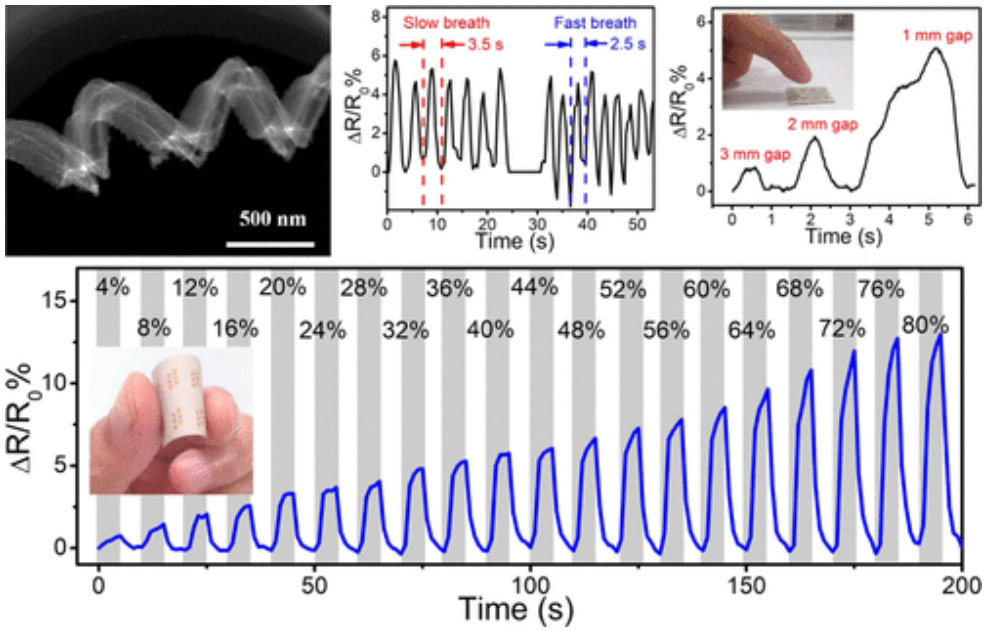

Figure 1.9 Structure, response time, sensitivity, and fingertip humidity measurement of the helical Carbon nanocoil humidity sensor, copied from the reference[41].

Liyun Ma et. al. developed a full-textile flexible wireless humidity sensor that can measure human respiration[42]. The unique hydrophobic property of the functional fibers makes the sensor has a faster response time of 3.5/4 s. The Unique fiber structure and yarn sensor make the sensor to be able to bend, twist, and stretched. Figure 1.10 shows the basic properties of the textile humidity sensor.

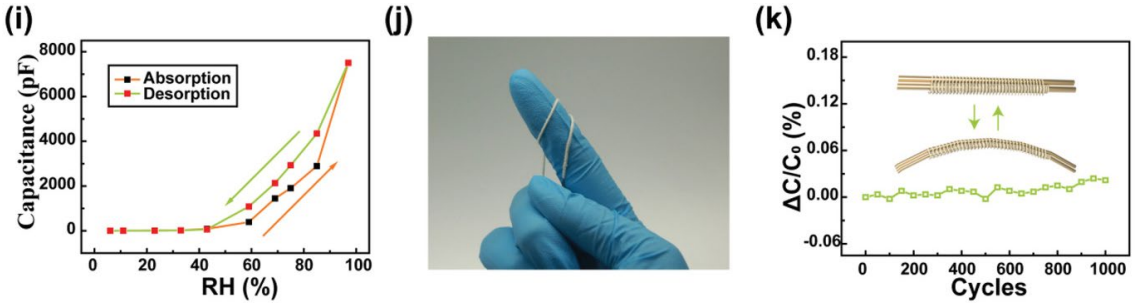

Figure 1.10 The sensitivity, flexibility, and bendability of the textile humidity sensor, copied from the reference[42].

1.4.2 High sensitivity

Human skin has a distribution of different humidity levels at different positions on the human skin surface. During daily activities, the skin humidity sometimes exhibits a tiny humidity change of less than 5% RH, such as during eating, or grasping objects [22]. Increasing humidity sensor sensitivity helps to improve the detection of the tiny change in skin humidity change, and also relieves the design of the supplementary circuits. Especially, the increasing of the sensitivity in the 40-100% RH range is of great importance. The biomedical measurements usually show a result lying in this range. For example, the back of human has a humidity changing from 60% RH to 100% RH. The fingertip exhibits a humidity range of 40-80% RH[22, 29]. Different works tried to improve the sensitivity and the detection limit of humidity.

Ning Li et. al. tried a method of growing TiO2 nanowires on a two-dimensional Ti_3C_2 MXene membrane. Increased sensitivity of higher than 1,000% in the range of 40%-100% RH was realized[43]. The increase in the sensitivity value is mainly due to the increase of the surface area, and the greater number of hydrophilic sites that can

improve the ability of absorption of water molecules. Figure 1.11 shows the structure of the materials and the resulted sensitivity.

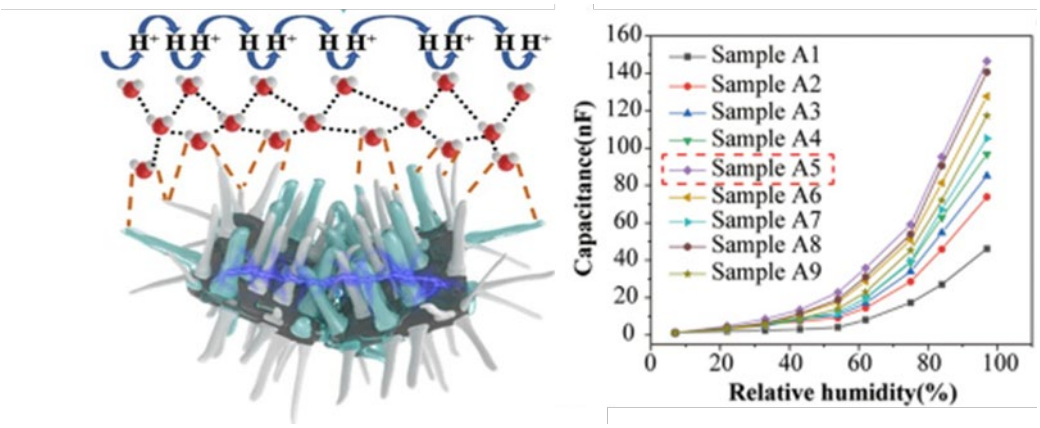

Figure 1.11 The illustration of the sensor materials and the sensitivity of the MXene humidity sensor, copied from the reference[43].

Jin Zhou et. al. reported a Polysquaraine-based humidity sensor with a high sensitivity of over 100 000% in the range of 40–100% RH were reported, as shown in Figure 1.12. The surface modification using Au nanoparticles improved the sensor's response to humidity as shown in the work.

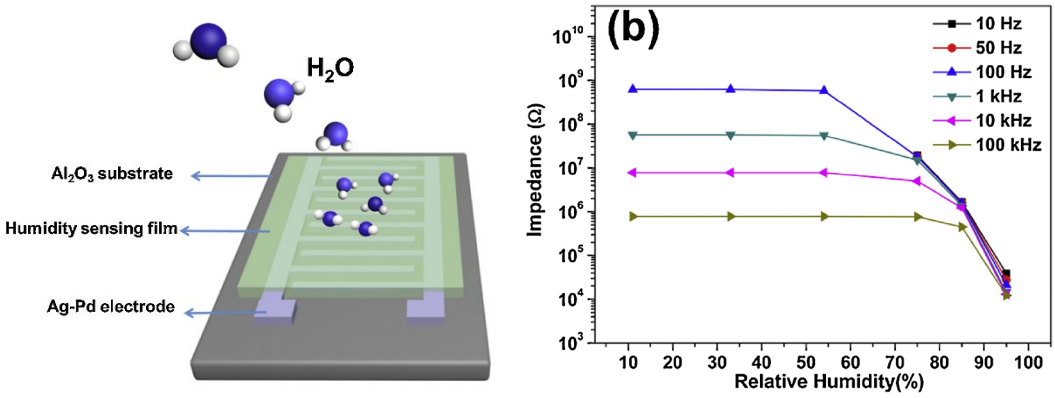

Figure 1.12 The illustration of the Polysquaraine-based humidity sensor and the resulting sensitivity, copied from the reference [44].

1.4.3 Gas-permeability

In addition to flexibility and high sensitivity, gas permeability is also needed for the long-term monitoring of wearable sensors to suppress the possibility of inflammation

and hair loss caused by skin sweating. Skin humidity with a range of 40–100% RH is higher when compared with the general air humidity, which raises a requirement for the skin-attachable sensors to have a high gas permeability for natural sweat evaporation. At the same time, gas-permeable sensors can avoid the accumulation of water on the sensor surface, which makes the sensor to be natural as bare human skin[36]. Recently, a gas-permeable nanomesh humidity sensor using parylene-coated polyvinyl alcohol (PVA) nanofibers was reported, which can perform continuous measurement of human skin humidity over a period of minutes[29]. The absorption of water expands the volume of material and makes cracks on gold electrodes, which works as a resistive-type sensor with a limited sensitivity of 25% in the range of 40–100% RH. Figure 1.13 shows the image of the sensor and the monitoring of skin humidity. For gas-permeable sensors, the increase of sensitivity of the sensor still remains a challenge.

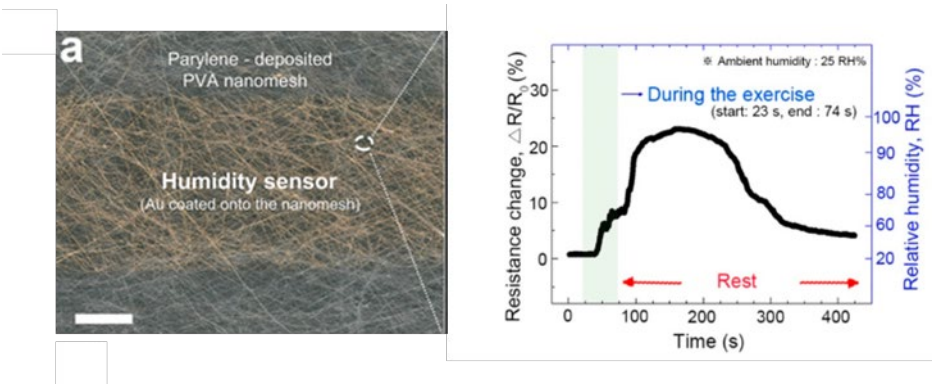

Figure 1.13 The illustration of the gas-permeable nanomesh humidity sensor and the monitoring of skin humidity during the exercise, copied from the reference[29].

1.5 Remaining issues of humidity sensors for skin health monitoring

The development of a highly sensitive humidity sensor with gas permeability that can be attached to human skin still remains a challenge, which is the main obstacle for on-skin humidity measurement. Highly sensitive materials are conventionally fabricated on continuous film-like substrates. As a result, the attachment of the sensors changes the skin humidity, which makes it difficult to accurately monitor inherent skin humidity. In the case of porous and ultrathin film sensors, the humidity response is usually due to

water absorption and cracks in the conductive layer, which limits the sensitivity. It has been required to realize highly sensitive porous humidity-sensitive materials and/or to optimize the structures, along with the integration of porous conductors and porous humidity-sensitive layers.

1.6 Purpose of this research

In this work, the research objective is to develop a flexible, highly sensitive, gas-permeable humidity sensor that can be attached to the skin for long-term monitoring. The flexibility makes the sensor possible to have a conformal attachment on the skin surface, a bending radius of less than 2 cm is needed for realizing the attachment on the human skin surface. Gas-permeability avoids sweat accumulation for realizing long-term monitoring, the value of gas-permeability should be able to allow the evaporation of sweat naturally, which requires a water vapor transmission rate of larger than 0.5 kg m^{-2} d^{-1}. High sensitivity increases the detectivity of the sensor, especially under a high humidity value.

1.7 Synopsis of this thesis

In chapter 1, the background of the on-skin wearable sensors and the humidity sensors are presented and discussed. The basic knowledge of humidity and its relationship with human health was introduced. The previous works of flexible humidity sensors are introduced, and the remaining challenge for on-skin humidity monitoring was discussed. The research objective is explained.

In chapter 2, the materials used in the fabrication were introduced, and the development of the nanomesh humidity sensor was introduced and discussed. The process of fabricating nanomesh structure by high-voltage electrospinning and thermal evaporation was presented. The sensor structure and its influence on the sensor's properties were presented. The experiment setup was introduced.

In chapter 3, the humidity sensing characteristics of the sensor were concluded. First,

the Figure of merits of a sensor was introduced, including the sensitivity, sensitivity drift, and linearity. Then the sensor properties are reported, including sensitivity, variations, hysteresis, and response time. Then the gas-permeability of the sensor was tested and shown. A long-term operation experiment result shows the stability of the sensor. Different structures' influence on the sensor was concluded.

In chapter 4, the mechanical and environmental durability was concluded. First, the sensor performance under mechanical deformations like pressing and bending were presented. The sensor's ability for continuous operation under the mechanical influence was confirmed. Then the sensor's performance under friction was also tested to confirm the ability to work on skin conditions. The stretchability test of 20% strain was shown. The temperature influence on the sensor was confirmed.

In chapter 5, the circuit model and impedance analysis of the sensor was introduced. First, the principle for the complex impedance analysis was introduced, Next, the impedance fitting result of the bode diagram and Nyquist diagram was concluded. The change of capacitor and resistor components results was introduced and discussed.

In chapter 6, the human skin humidity measurement results were shown. The distribution of humidity at different positions of human skin was presented, then a one-hour continuous measurement of human skin measurement with exercise was shown.

2. Fabrication of nanomesh humidity sensor

2.1 Materials

2.1.1 PVA

Polyvinyl alcohol (PVA) is one of the most commonly used bio-compatible polymers that can be used in various medical applications. The low tendency for protein adhesion, low toxicity, and water-solubility make it suitable as a component touching bio-tissues. Cartilage replacements, contact lenses, and eye drop usually use PVA as material.

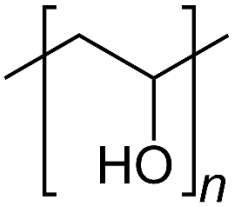

Figure 2.1 Chemical structure of polyvinyl alcohol

The conductivity of PVA at 303K is 5.62×10^{-10} S/cm, which is usually considered an insulator.[45] The conductivity of PVA can be enhanced by modifications of doping with other conductive materials like polyaniline[46], Au[47], and ZnO[48]. More importantly, PVA contains hydroxyl which makes it easy to combine with water molecules and absorb water vapor. The absorption of water contributes to the enhancement of conductivity and change of permeability, which makes humidity sensitivity.

In this work, PVA powder (EG-22P) was purchased from Nippon Synthetic Chemical Industries for fabrication. The PVA solution was prepared by dissolving PVA powder into the water with 10 wt%. The PVA was used as sensitive material, which is laminated on the two sides of the PU nanomesh. Also, the partially dissolved PVA forms adhesion between different nanomesh layers and between the sensor and human skin.

2.1.2 PU

Polyurethane (PU) refers to a class of polymers composed of organic units joined by

urethane links.

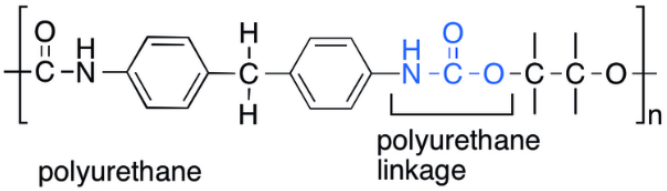

Figure 2.2 Chemical structure of polyurethane

Compared with PVA, pure PU has lower electrical conductivity, which is between 10^{-14} S/cm to 10^{-10} S/cm[49]. Pure PU is hydrophobic in nature and insoluble in water[50]. The property of PU makes it insensitive to the water molecule.

In this work, a pristine PU solution (Rezamin ME-8115LP, 30 wt%) was purchased from Dainichiseika for use. N,N-dimethylformamide (DMF), methyl ethyl ketone (MEK) were purchased from FUJIFILM Wako Pure Chemical Corporation as solvents for PU solution. The polyurethane solution (15 wt%) was prepared by diluting the pristine PU solution with a mixture of DMF and MEK (wt/wt = 7:3). The PU material was used as an insulator layer and scaffold for the sensor. Without the existence of the PU nanomesh layer, the top and bottom electrodes will easily form short-circuit.

2.1.3 Metal salts for controlling humidities

In this work, different kinds of saturated salt solutions are used to keep the humidity value constant in the sealed bottles[51].

NaCl (sodium chloride, ≥99.0%) was purchased from Merck KGaA Sigma–Aldrich. CaCl2 (calcium chloride, anhydrous, ≥95.0%), CH3COOK (potassium acetate, ≥97.0%), MgCl2 (magnesium chloride, anhydrous), K2CO3 (potassium carbonate, anhydrous, ≥99.5%), Mg(NO3)2·6H2O (magnesium nitrate, ≥9.0%), CuCl2 (copper(II) chloride, ≥99.0%), KCl (potassium chloride, ≥99.0%), and K2SO4 (potassium sulfate, ≥99.0%) were purchased from FUJIFILM Wako Pure Chemical Corporation. 150 g of $CaCl_2$, 200 g of CH_3COOK, 200 g of $MgCl_2$, 300 g of K_2CO_3, 200 g of $Mg(NO_3)_2 \cdot 6H_2O$,

200 g of $CuCl_2$, 200 g of NaCl, 60 g of KCl, and 250 g of K_2SO_4 were dissolved respectively in 150 mL pure water to prepare the saturated solutions.

The solution volumes exceeded half the size of the bottles. The relative humidity values in the bottles were 9%, 23%, 33%, 43%, 54%, 67%, 75%, 84%, and 97%, respectively.

2.2 Nanomesh structure and its preparation

2.2.1 Multilayer structure

As shown in figure 2.3. The as-prepared sensor has a multilayer nanomesh porous structure. In the middle of the sensor, a 2cm*2cm size PU nanomesh layer was used as the insulator and scaffold of the sensor. On the top and bottom side two 2cm*2cm size PVA nanomesh layers were attached to the PU nanomesh layer, which works as the sensitive layer. The patterned Au of 0.5cm * 2cm size was deposited on the surface of the PVA nanomesh layer as electrodes. The adhesion of the multiple layers is formed by partially-dissolved PVA.

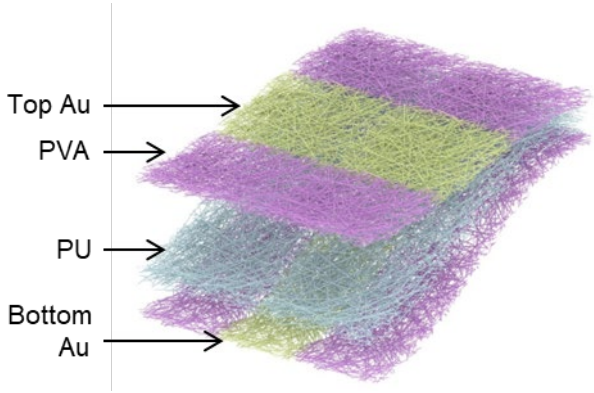

Figure 2.3 Multilayer structure of the nanomesh humidity sensor

2.2.2 Electrospinning fabrication method

The nanomesh structure was prepared by the high voltage electrospinning method. The setup for the electrospinning process is shown in Figure 2.4. A syringe contains the polymer solutions and is placed on top of a metal roller. A high voltage is added between the needle of the syringe and the roller. A silicone-coated paper is attached to the roller

to collect the fibers. During the electrospinning process, the polymer solution was sprayed out from the syringe, and a Tylor cone was formed by the repulsive force of static charge. The high voltage drives the solution to the metal roller. Then fibers with random directions are collected. After the solvent evaporates, the polymer fibers with a diameter of several hundred nanometers to several micrometers form on the surface of the roller.

In this work, a 20 kV voltage was applied to the setup, and the distance between the needle tip and the collector was 20 cm. For fabrication of PVA nanofibers, a 1.0 mL/h feed rate was applied to the syringe feeding controller, and 48 min of electrospinning time was applied to reach a satisfying thickness. For fabrication of PU nanofibers, 0.8 mL/h feed rate was applied to the syringe feeding controller, and 2 hours of electrospinning time was applied to reach a satisfying thickness.

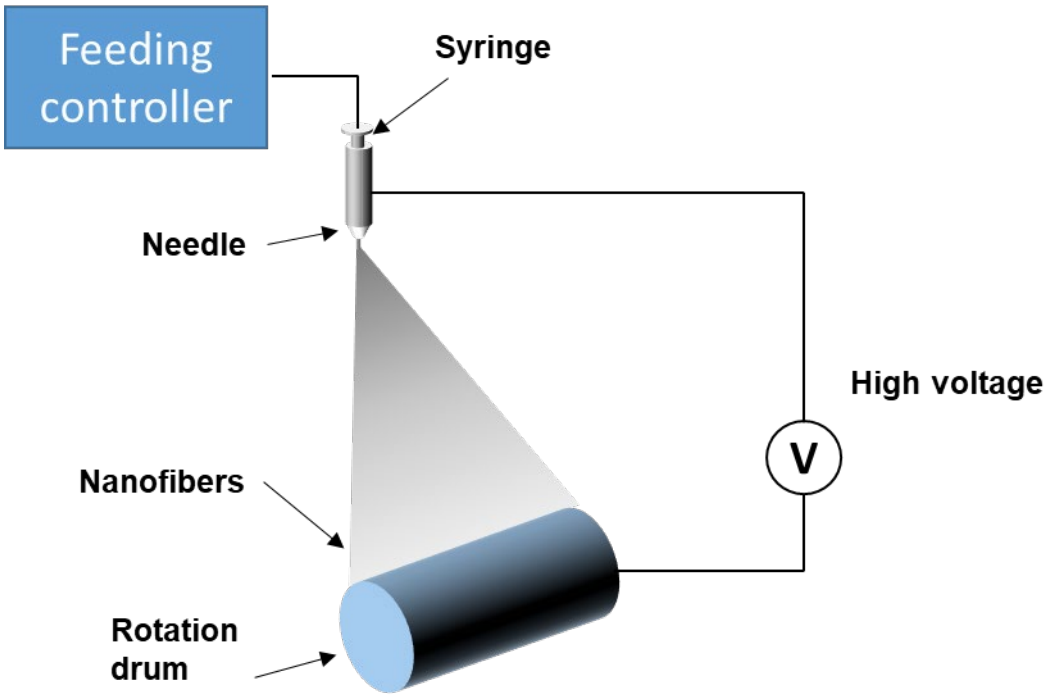

Figure 2.4 The setup for the electrospinning method

2.2.3 Nanomesh porous structure

The SEM images of the as-prepared PVA and PU nanofibers are shown in Figure 2.5. The nanofibers cross each other and form a nanomesh sheet. The nanomesh sheet shows

a porous structure, which is an important property that makes the nanomesh sheet able to contain gas-permeability.

The PVA nanomesh has a mean diameter value of 0.344 ± 0.079 μm and a density of 0.047 mg/cm^2. On the other hand, the PU nanomesh has a mean diameter value of 0.566 ± 0.197 μm and a density of 0.342 mg/cm^2. It is easy to distinguish that the PU nanofibers have a larger mean diameter and a higher density.

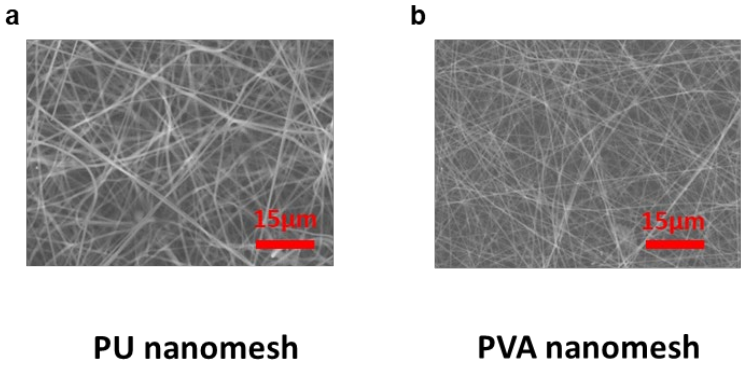

Figure 2.5 SEM images of the surface of PU nanomesh and PVA nanomesh.

2.3 Lamination of nanomesh sheets

After obtaining the PVA and PU nanomesh sheets, 100nm thick Au was deposited on the surface of the PVA nanomesh by the heated evaporator. The Au electrode was patterned using a shadowed mask and the formed electrode has a size of 0.5cm*2cm.

The obtained nanomesh sheets are extremely soft and easily broken during the flowing transfer and lamination process. To temporarily hold the nanomesh sheet, a 125 μm polyimide (PI) frame was used as a supporting substrate. The 125 μm PI film was patterned using a laser cutter to have a window of 2cm*2cm. The opened window decides the sensor size.

During the formation of the multiple layer structure, first, a PU nanomesh sheet was laminated onto the frame, forming a freestanding sheet on the open area. Then, two Au-deposited PVA nanomesh layers were attached to both sides of the open area of the PU nanomesh, and ethanol was applied to the surface of the nanomesh after it. The partially

dissolved PVA can form in the pores of PU nanomesh and provides adhesion between the three nanomesh layers. The whole lamination process can be shown in Figure 2.6.

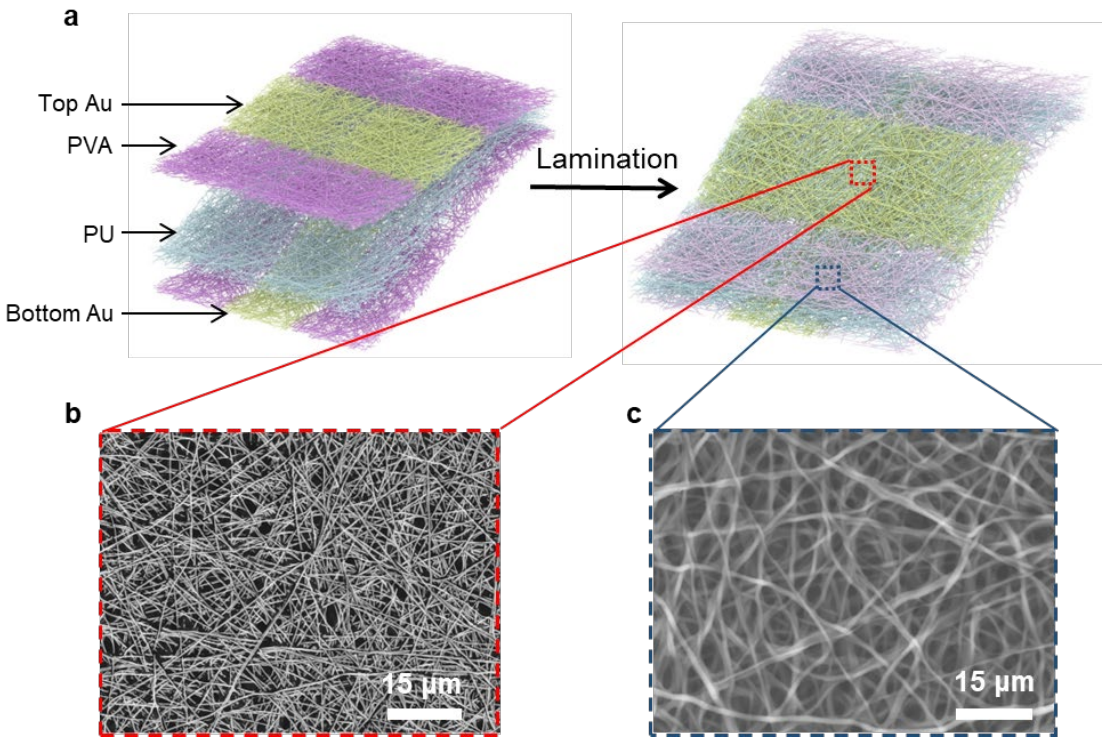

Figure 2.6 Lamination of the nanomesh humidity sensor. a) Schematic of the multilayer sandwich structure of the nanomesh sensor before and after the lamination. b) Porous crossing structure of the nanomesh Au electrode. c) Porous crossing structure of the PU nanomesh.

By lamination of multiple nanomesh sheets, the nanomesh humidity sensor forms. The whole sensor shows a sandwiched three-layer structure. As shown in Figure 2.7, in the cross-sectional SEM image, the top and bottom layers show Au coating with bright color, and between the top and bottom electrodes, the middle layer contains PU nanofibers with PVA coatings.

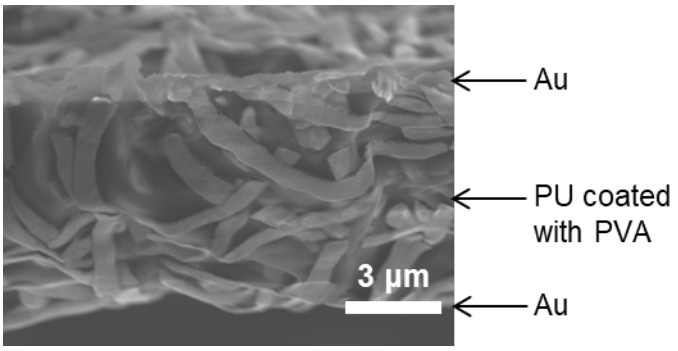

Figure 2.7 The cross-sectional SEM image of the multilayer structure

After laminating, the sensor exhibits partially dissolved PVA on the sensor surface. By further dissolving PVA nanomesh on the skin, or simply applying ethanol to the human skin surface, it is easy to form a conformable attachment with the skin, as shown in Figure 2.8.

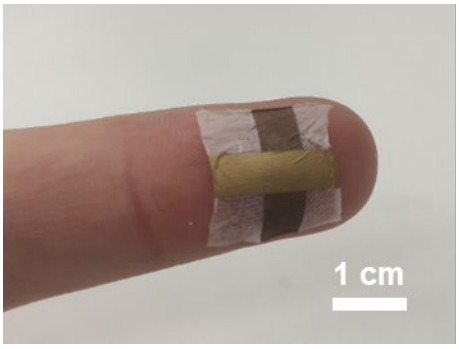

Figure 2.8 The photo showing the conformable attachment of the nanomesh humidity sensor to human skin.

2.4 Experiment setup

In this work, we measured the impedance of the nanomesh humidity sensor to indicate the humidity sensitivity. We attached the thin connection wires on the surface of the Au electrode surface by medical tape for the measurement. The impedance amplitude and impedance angle were measured using an LCR meter (Agilent 4284A). The AC current is recorded by applying an AC voltage to the test device. Impedance is calculated by dividing the voltage magnitude by the current magnitude. The frequency of the applied voltage is 20–10,000 Hz and the amplitude is 100 mV.

Two methods were used for the control and maintaining of the humidity: First, by using a temperature and humidity cabinet; second, the use of different saturated solutions in airtight bottles. Photographs of the measurement setup are presented in Figure 2.9.

In the first method, a temperature and humidity cabinet (LUH-113, ESPEC) was used to control and maintain the humidity. The humidity range was limited to 60%–100%. A temperature of 25–50 °C was used to test the sensor performance at different temperatures.

In the second method, different saturated salt solutions were used to maintain a certain relative-humidity level in an airtight environment. CaCl2, CH3COOK, MgCl2, K2CO3, Mg(NO3)2, CuCl2, NaCl, KCl, and K2SO4 were dissolved in pure water to prepare the saturated salt solutions, which were contained in airtight bottles with a size of 1 L (HARIO). The solution volumes exceeded half the size of the bottles. The relative humidity values in the bottles were 9%, 23%, 33%, 43%, 54%, 67%, 75%, 84%, and 97%, respectively. This method can be used to measure the sensor impedance at low humidity levels.

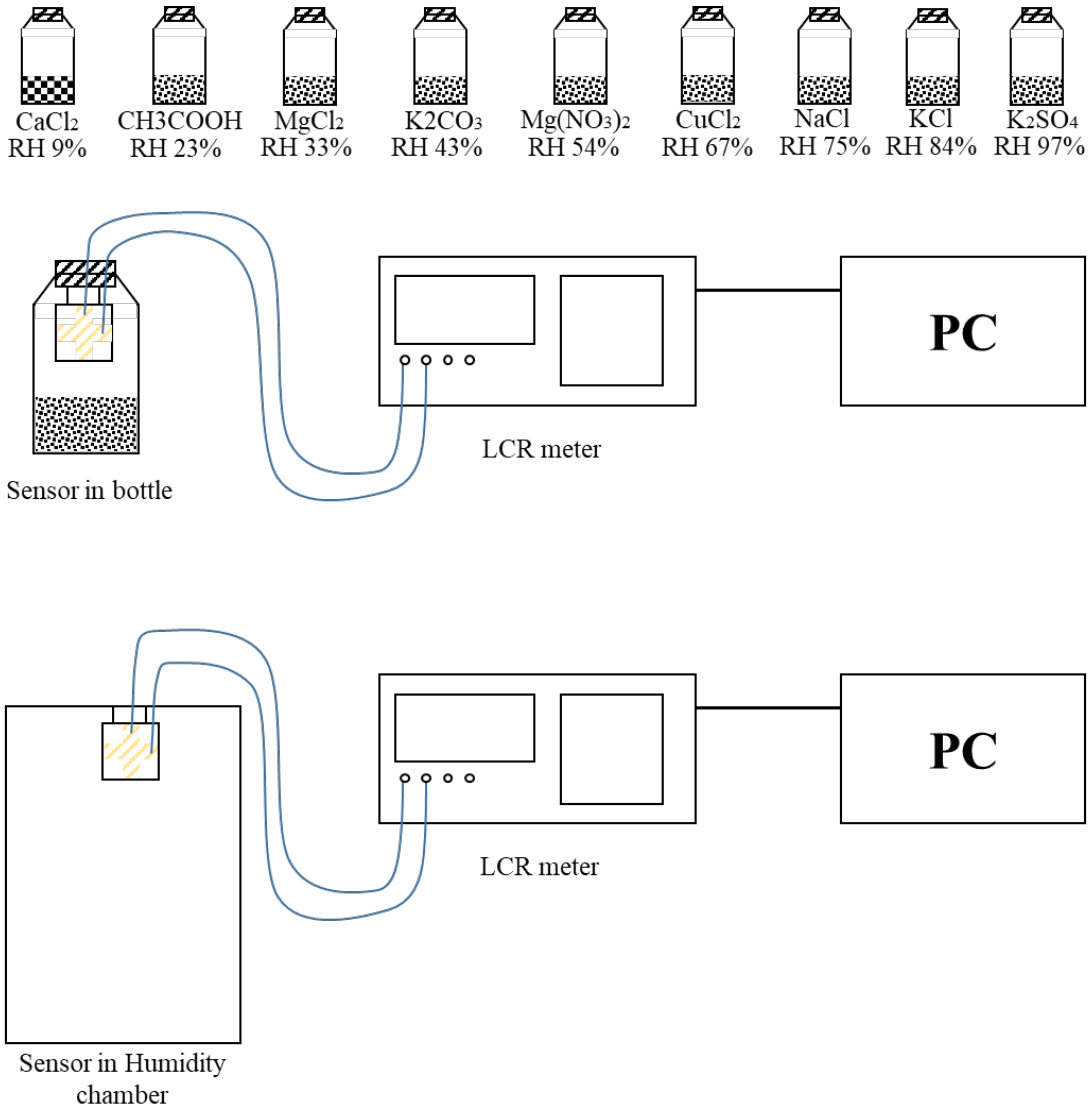

Figure 2.9 The measurement setup with two different methods to control the humidity.

The measurement of human skin humidity was achieved through conformable attachment of the nanomesh humidity sensor to the skin. The freestanding nanomesh humidity sensor was placed on the skin surface, and ethanol was used to make the sensor flat and adhesive to the skin. Additionally, a commercial humidity sensor (DHT 11) was attached to the skin using medical tape, and the humidity and temperature were measured together. For the skin test, the study protocol was thoroughly reviewed and approved by the ethical committee of The University of Tokyo (approval no. KE19-32), and informed consent was obtained from all participants for all experiments. The measurement situation was shown in Figure 2.10.

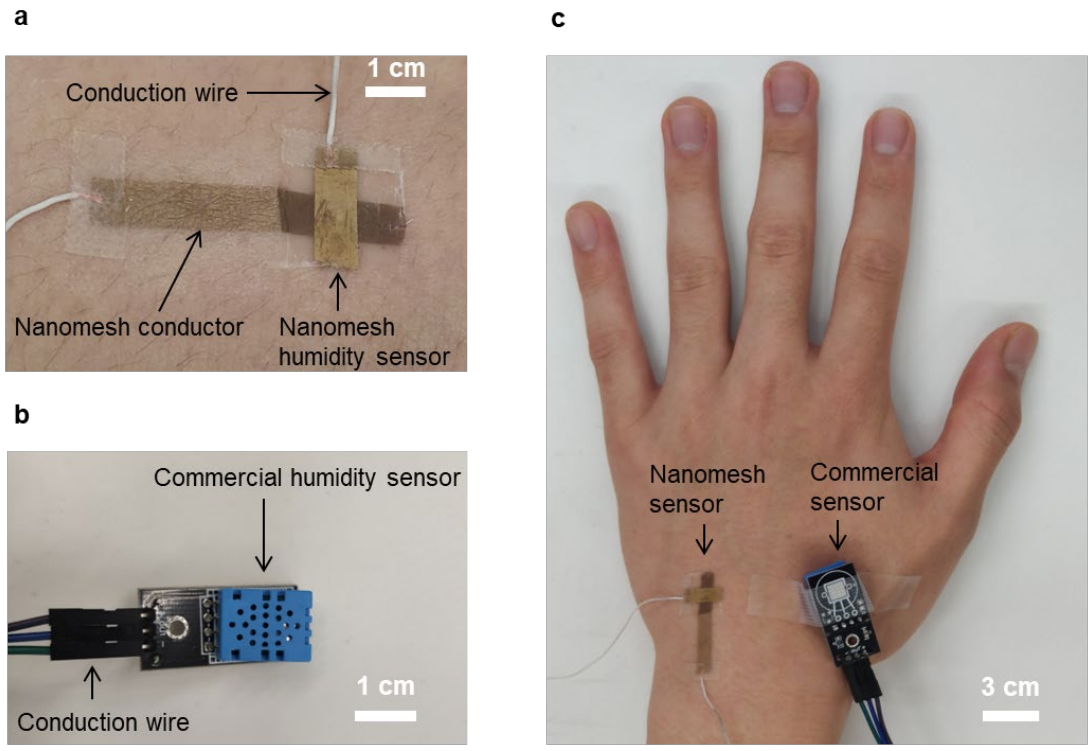

Figure 2.10 Photos of the nanomesh humidity sensor and commercial humidity sensor. a) The attachment of nanomesh humidity sensor on skin. b) Shape of the commercial humidity sensor. c) Monitoring of skin humidity using both nanomesh humidity sensor and commercial humidity sensor.

3. Humidity sensing characteristics

3.1 Figures of merit for a sensor

To enable the users to compare the performance of sensors quantitatively and decide the availability of specified applications, clearly defined criteria are needed. Usually, two kinds of characteristics are needed to be considered, depending on the frequency of the input signals[52, 53].

Static characteristics: The performance of sensors for DC or very low-frequency inputs is described by static characteristics. The properties of output for a constant input show the quality of the sensor, including the response itself and the linear, statistical effects.

Dynamic characteristics: The performance of sensors under high frequencies can be described. The dynamic performance shows the sensing property with time-varying information. The use of differential equations to describe the sensing properties is usually needed.

The following table shows the typical range and different frequencies of some commonly seen bio-signals[53].

Table 3.1. The typical signal range and frequency range of the typical bio-signals

Bio signal	**Typical signal range**	**Frequency range, Hz**	**Standard sensor**
Blood pressure, arterial	10-400 mm Hg	dc-50	Strain-gage manometer
Blood pressure, venous	0-50 mm Hg	dc-50	Strain gage
P_{O2}	30-100 mm Hg	dc-2	Specific electrode
Skin pH	4-6 pH units	dc-2	Specific electrode
Skin humidity	30-100% RH	dc-0.1	Polymer, metal oxide sensors
Body temperature	32-40℃	dc-0.1	Thermistor, Thermocouple

The skin humidity is a typical near DC signal. Usually, static characteristics are firstly required to describe the sensor properties.

3.1.1 Static sensitivity

Static sensitivity is measured by controlling all inputs to be constant except only one. The one input is varied incrementally over the defined sensor input range and leads to the response of the sensor in an incremental output. The static sensitivity can be regarded as the slope of the input-output curve. In the linear range, the static sensitivity can be constant. The slope and intercept of the sensor can be calculated by:

$$m = \frac{n\sum x_i y_i - (\sum x_i)(\sum y_i)}{n\sum x_i^2 - (\sum x_i)^2} \quad (4)$$

$$b = \frac{(\sum y_i)(\sum x_i^2) - (\sum x_i y_i)(\sum x_i)}{n\sum x_i^2 - (\sum x_i)^2} \quad (5)$$

$$y = mx + b \quad (6)$$

Where n is the number of points and each sum is for all n points.

3.1.2 Zero drift and Sensitivity drift

Zero drift refers to the overall increase or decrease of the data points by an absolute amount, while the slope of the curve (which usually refers to the sensitivity). Many factors can contribute to zero drift: fabrication misalignment, ambient temperature variation, hysteresis, and vibration. In addition to the zero drift, the sensitivity curve also exhibits sensitivity drift, which is defined as the increase or decrease of the slope of the input-output curve. Same as zero drift, sensitivity drift also results from fabrication variations and changes in ambient temperature, and apart from that, the variations in power supply and nonlinearities also influence the sensitivity value. Figure 3.1 shows the zero drift and sensitivity drift.

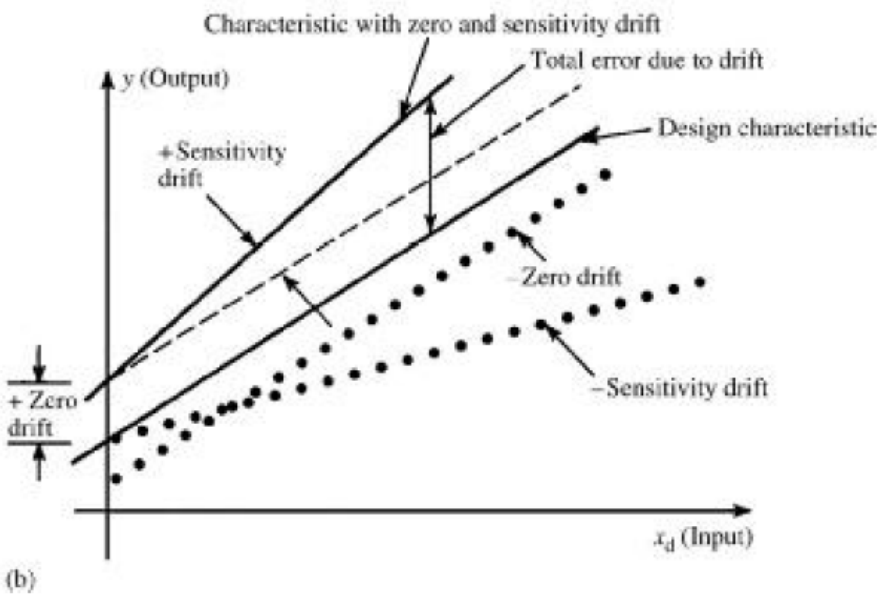

Figure 3.1 Zero drift and sensitivity drift. The dotted line means the zero drift and sensitivity drift can be negative, copied from reference[52].

3.1.3 Linearity

The linear system fulfills the requirements of additivity and homogeneity of degree. It can be explained as the following figure:

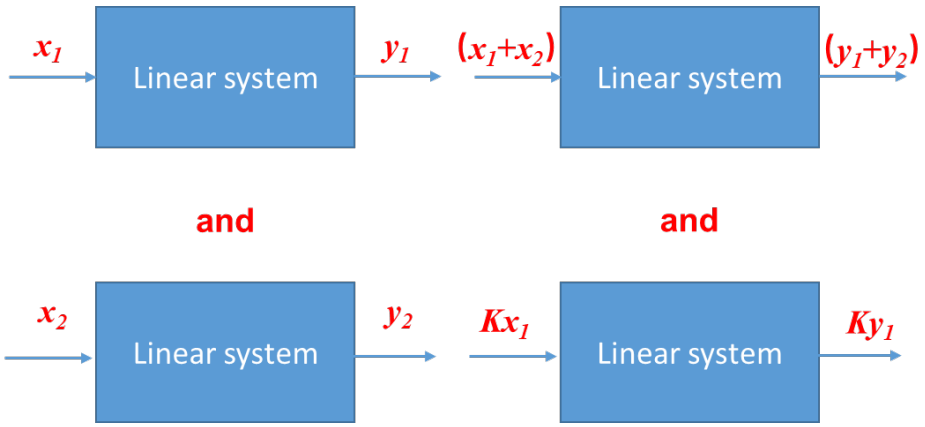

Figure 3.2 The linearity of a system, including superposition and homogeneity

The two features of the linear system are shown in this figure. One is the superposition property, which means the adding of input x_1 and x_2 will lead to the adding of output y_1 and y_2. Another feature is homogeneity, the multiplexing with K to the input will lead to the multiplexing of output with K.

3.2 Wettability of nanomesh structure

Wettability usually refers to the ability of a liquid to maintain contact with a solid surface[54]. The wettability depends on the molecular interactions between water and solid. The wettability is usually measured by the contact angle, which is the angle between the interface of the solid surface and the liquid. The contact angle quantifies the wettability by the Young equation, when the contact angle is less than 90°, the surface of a solid has a wettable surface, also termed as hydrophilic; when the contact angle is greater than 90°, the surface of the solid has a non-wettable surface and also called hydrophobically.

Young equation considers the thermodynamic equilibrium between the three phases of liquid(L), solid(S), and gas (G):

$$\gamma_{SG} - \gamma_{SL} - \gamma_{LG} cos\theta_c = 0 \quad (7)$$

Here, γ_{SG} is the solid-vapor interfacial energy, γ_{SL} is the solid-liquid interfacial energy, and γ_{LG} is the liquid-vapor interfacial energy like the surface tension. Then the equilibrium contact angle is calculated through the Young equation.

The contact angle is related to the water absorption and swelling functions. As already shown in section 1.2.2, the capillary effect is dependent on the wettability of the materials. When the contact angle decreases and becomes more hydrophilic, the value of Kelvin radius increases, making more pores in the polymer structure become able to be filled with water molecules, and the ability to absorb water increases.

In this work, the PU nanomesh and PVA nanomesh were fabricated and utilized. The basic wettability of the two different nanomesh materials was measured.

PU nanomesh is a hydrophobic porous layer, that usually contains a contact angle larger than 90°. The PU nanomesh was fabricated with a solution feeding rate of 1.2 mL/h and an electrospinning time of 1 hour was prepared. Figure 3.3 shows the measured contact angle of the PU nanomesh right after the contact between water drop and film. The contact of the PU nanomesh sheet shows a hydrophobic property of 122.7°, which

makes it repel moisture. The PU property makes it not absorbing of water and maintains stability as the middle frame as the sensor.

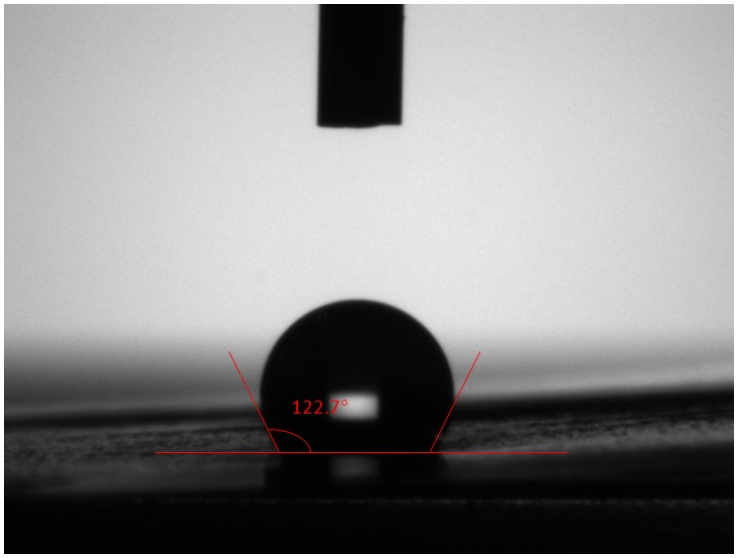

Figure 3.3 The contact angle of the PU nanomesh sheet

At the same, the time-varying value of the contact angle of the PU nanomesh sheet was measured, as shown in Figure 3.4. The PU nanomesh shows a quasi-stable contact angle in 35s. The contact angle shows no obvious decreasing trend. This property proves that the PU nanomesh does not dissolve in water and shows no absorption or swelling effect.

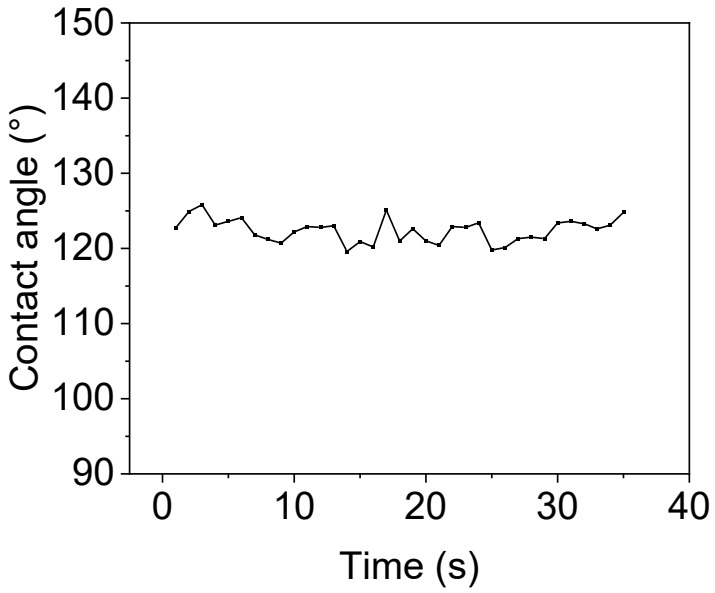

Figure 3.4 Time-varying property of the contact angle of PU nanomesh

Next, the nanomesh PVA nanomesh sheet was contacted with water drop, and the contact angle was measured. The PVA nanomesh fabricated with a solution feeding rate of 1.2 mL/h and electrospinning time of 20 min was prepared. Figure 3.5 shows the measured contact angle of the PVA nanomesh right after the contact between water drop and film. The contact of the PVA nanomesh sheet shows a hydrophilic property of 59.5°, which makes it able to absorb moisture.

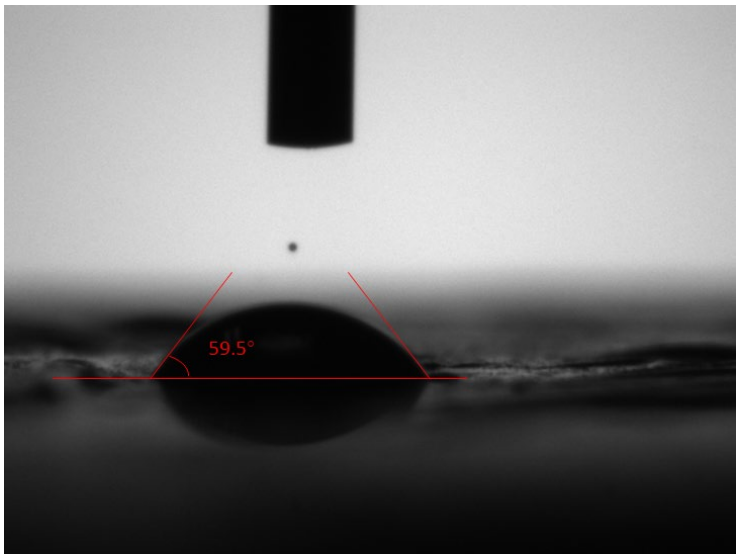

Figure 3.5 The contact angle of the PVA nanomesh sheet

Also, Figure 3.6 shows the time-varying value of the contact angle of the PVA nanomesh sheet. The PVA nanomesh shows a decreasing trend of contact angle, which is different from the PU nanomesh. The decreasing of the contact angle is caused by the absorption and swelling effect of the PVA material, which shows the PVA's ability to absorption of water.

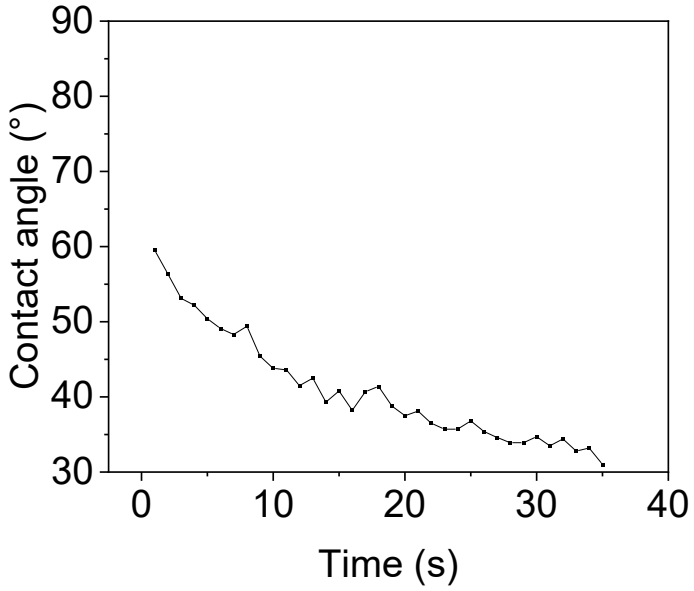

Figure 3.6 Time-varying property of the contact angle of PVA nanomesh

3.3 Nanomesh humidity sensor properties

3.3.1 Sensitivity

The sensitivity of the sensor is usually defined as how much its output changes when the input quantity it measures changes. The relative change can be defined as equation (8):

$$S_r = \frac{\Delta y/y_0}{\Delta x/x_0} \tag{8}$$

Where S_r is the relative value-based sensitivity over a certain input range, Δx is a certain change of the input value in the considered range, x_0 is the initial input value. Δy is the output value change over the input value change of Δx, y_0 is the initial output value at the input of x_0.

Also, sensitivity can be defined as equation (9) by the ratio of the absolute changing:

$$S_a = \frac{\Delta y}{\Delta x} \tag{9}$$

Where S_a is the absolute value-based sensitivity over a certain input range, Δx is a certain change of the input value in the considered range. Δy is the output value

change over the input value change of Δx.

In the case when the output change and input change have a linear relationship, the sensitivity defined by equation (8) or (9) shows the slope of the curve.

$$y = ax + b \tag{10}$$

Where a and b are constants.

For example, in equation (7) the absolute sensitivity results will be:

$$S_a = \frac{\Delta y}{\Delta x} = a \tag{11}$$

Which will be a constant value. And the relative changing ratio will be:

$$S_r = \frac{\Delta y/y_0}{\Delta x/x_0} = a\frac{x_0}{y_0} \tag{12}$$

Which is also a constant value. The value is the slope divided by the ratio of initial output and input values. It can be seen as a normalized value of absolute sensitivity, which has a unit of 1.

In this work, however, the response of the humidity sensor to the humidity is not always a linear function. So, if the sensitivity is defined by the conventional method, the humidity sensor does not maintain a constant sensitivity over the whole humidity range. But the in this work the sensor output shows an exponential relationship with the input value in a certain input range. As shown in the following equation.

$$Z = a \times b^{RH} \tag{13}$$

Here a and b are constants, Z is the impedance of the sensor, RH is the relative humidity value. In such a case, if the graph of Z versus RH is plotted, the slope will be a constant:

$$\ln Z = \ln a + \ln b \times RH \tag{14}$$

In such a case, we define the sensitivity in this work as the relative change ratio over a certain change of humidity:

$$S = \frac{(Z_{max} - Z_{min})}{Z_{min}} \tag{15}$$

where $\boldsymbol{S}$ is the sensitivity over a certain humidity change, $\boldsymbol{Z_{max}}$ is the maximum impedance in the considered humidity range, and $\boldsymbol{Z_{min}}$ is the minimum impedance in the considered humidity range. The value of $\boldsymbol{S}$ is related to the humidity change. Only when the humidity change value is the same, $\boldsymbol{S}$ can be compared.

So, the sensitivity will be constant under the same humidity change $(RH_{max} - RH_{min})$:

$$S = \frac{(Z_{max} - Z_{min})}{Z_{min}} = b^{(RH_{max} - RH_{min})} - 1 \tag{16}$$

The response of the humidity sensor to the humidity change is shown in figure 3.7.

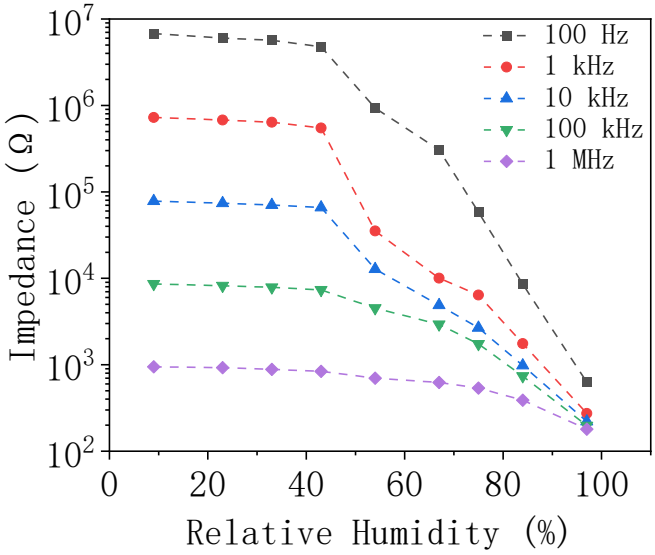

Figure 3.7 Sensor's response to the humidity change

As shown in Figure 3.7, the response of the sensor to humidity was measured in electrical impedance changes of the sensor over the two Au electrodes on the sensor surface. The response of the sensor comes from the conductive property and permittivity change of the sensitive structure. The absorption of water leads to both resistance and capacitance changes, as indicated by the impedance. The sensor exhibits two different sensitivity ranges: the low sensitivity range of 49-43% RH which was characterized by a linear relationship between the relative humidity and the impedance,

and the high sensitivity range of 43-97% RH, which was characterized by an exponential relationship between the relative humidity and the impedance.

A curve fitting of the sensitivity over the linear range (9% RH to 43% RH) and the exponential range (43% RH to 97% RH) was done and shown in Figure 3.8. The repeated response of the sensor from 9% RH to 97% RH and back again to 9% RH was shown in Figure 3.5.

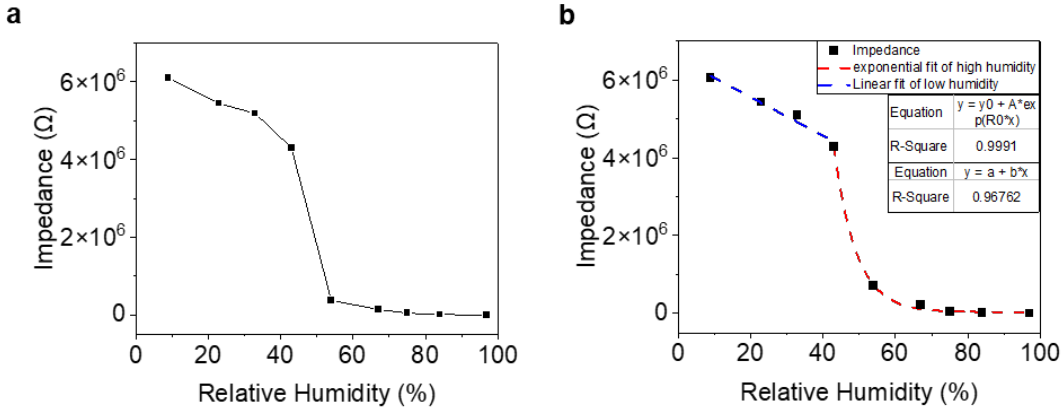

Figure 3.8 a) Sensitivity of nanomesh humidity sensor in liner scale. b) Fitting of the sensitivity in two ranges using Exponential curve and linear curve.

In the range of 9% RH to 43% RH, the impedance changed from 6.96MΩ to 3.21 MΩ. The data were fitted by a linear curve of $y = a + bx$. The R square value of the curve fitting is 0.96762. In the range of 43% RH to 97% RH, the impedance changed from 3.21 MΩ to 501 Ω, and the sensitivity was 640,000%/43%-97% RH. The data were fitted by the exponential curve $y = y_0 + Ae^x$, and the R square value of the curve fitting is 0.96762. According to the best of our knowledge, the sensitivity of the proposed sensor in this range is higher than or comparable to all previous results.

By plotting the curve of exponential relationship into the figure with a log scale in the y axis, the curve will show a linear relationship. As shown in Figure 3.9.

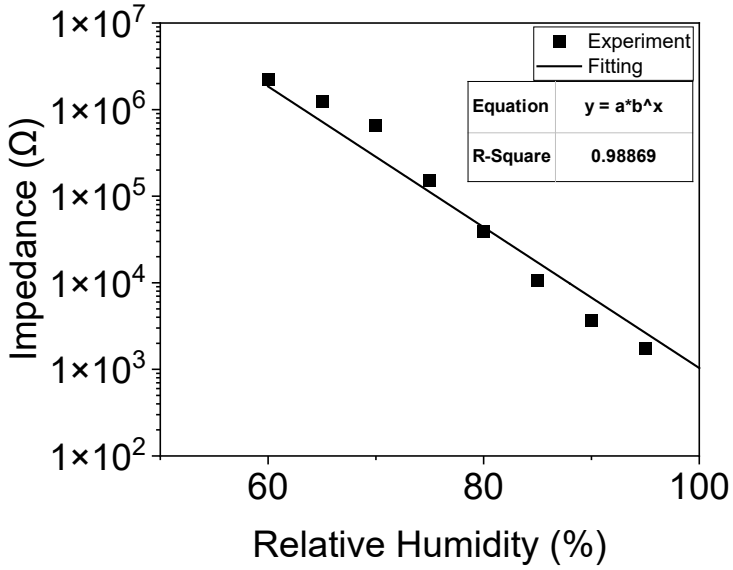

Figure 3.9 Fitting result of the impedance curve in the humidity from 60% to 100% RH using an exponential relationship between RH and impedance

The sensor exhibited different sensitivities at different frequencies. At higher frequencies, the sensor exhibited a smaller impedance change (946 Ω at 9% RH to 180 Ω at 97%, which was measured under 1 MHz). The impedance differences at various frequencies originated from the capacitive components in the equivalent circuit of the sensor, which is discussed in the following chapters. Then the frequency increased, and the impedance values contributed by the capacitive components decreased, which resulted in a lower impedance value of the whole sensor.

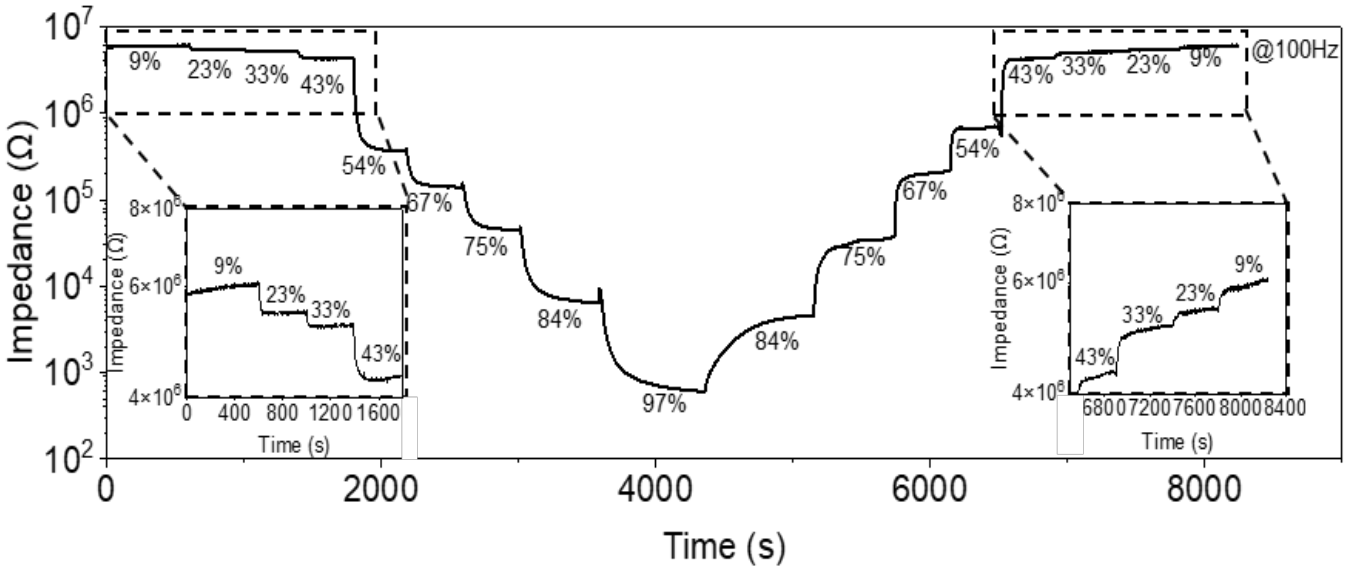

Figure 3.10 shows the sensor's cycle response from 9% to 97% RH, which was measured at 100 Hz. The sensor exhibited good reversibility over the wide humidity, and impedance changed over four orders of magnitude and the sensor exhibits good reversibility.

3.3.2 Variation of the humidity sensors

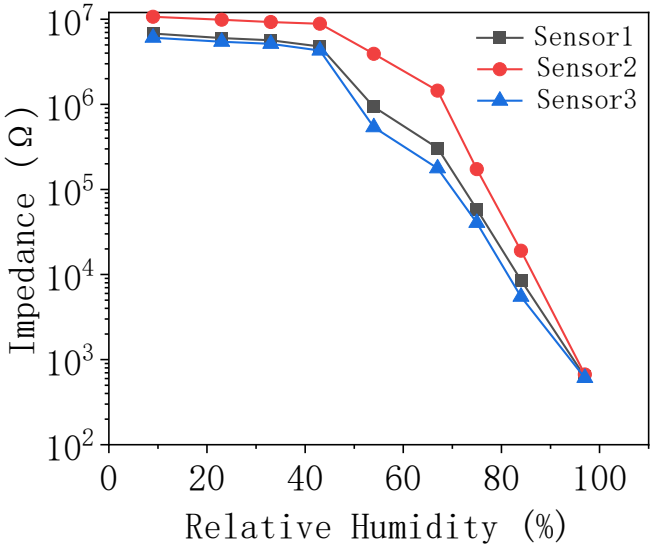

Figure 3.11 Variation of the sensitivity in different sensors

The sensors fabricated under the same conditions exhibit variations. The variation is small and less than an 8.9% difference. By normalization of the value by dividing the initial impedance value, the influence of the variation can be suppressed. Figure 3.11 shows the variation of the sensor.

3.3.3 Hysteresis

Hysteresis usually exists in the humidity sensors. Hysteresis means the difference in sensor output between increasing and decreasing humidity. Sensors with small hysteresis are useful for precise reading. In this work, the hysteresis of the sensor is defined by the difference in the slope of the sensitivity curve under the log scale. The origin of hysteresis is the asymmetric ability of absorption and desorption of water molecules.

In this work, an organic polymer (PVA) was used as a humidity-sensitive material. Hysteresis comes from the clusters of absorbed water inside the bulk polymer.[55, 56] The formation of clusters indicates that the hygroscopicity of some polymers is too high, and relatively large pores exist in the polymeric structures. The water clusters may also deform the polymers' structure due to the formation of ink-bottles-type pores in polymer materials and shorten the lifetimes of the sensors.

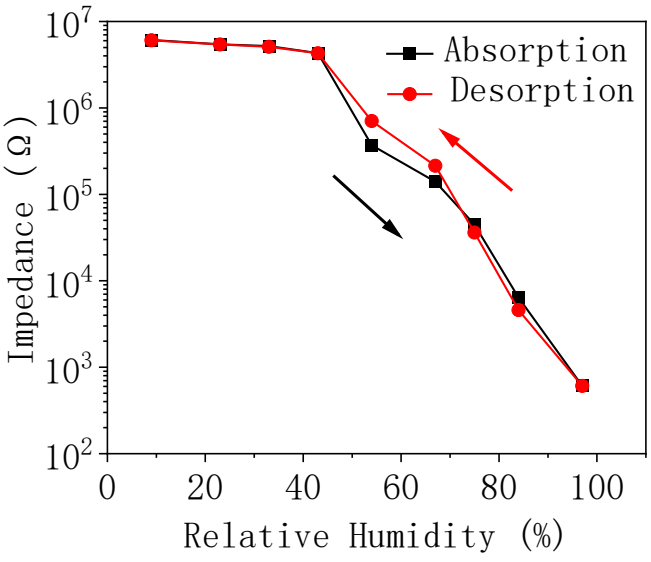

Figure 3.12 Hysteresis of the nanomesh humidity sensor.

Figure 3.12 shows the hysteresis of the nanomesh humidity sensor. The humidity sensor shows a hysteresis of less than 5.3%, by calculating the slope of the sensor.

3.3.4 Response time

The response time of the sensor is an important parameter. With a fast response time, the sensor is able to catch fast changes in skin humidity under skin monitoring. The response time of the sensor is shown in Figure 3.13.

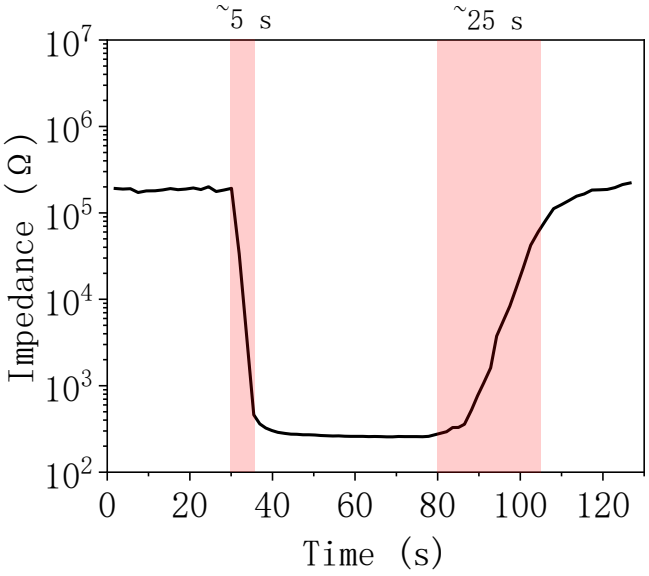

Figure 3.13 Response time of the humidity sensor under humidity increase and decrease

The response time was determined by the time interval required to reach 90% of the total impedance change. From 60% to 100% RH, the absorption time of the sensor was approximately 5 s, and the desorption time of the sensor was approximately 25 s. According to the typical signal frequency, the human skin humidity has a frequency from DC to 0.1 Hz. The response time of 5/25s is enough for most measurement cases.

3.4 Gas-permeability

The porous structure has good gas-permeability. In the experiments, we prepared four bottles each containing 1 g of water. The openings of three of the bottles were tightly sealed with the proposed sensor, 50-μm-thick PU film, and Al foil, and the remaining one bottle was kept open. The weight decreasing rate shown in Figure 3.14 was used to

describe the gas-permeability. The sensor had a water transmission rate of 0.957 kg/(m^2d), which was similar to the value of the open bottle (1.09 kg/(m^2d)). In comparison, the 100-μm-thick PU film had a gas-permeability of only 0.217 kg/(m^2d), and the Al foil had almost no gas-permeability. The natural water evaporation rate on human skin is approximately 0.5 kg/(m^2d); thus, the sensor can maintain a natural sweat outflow when applied to the skin.

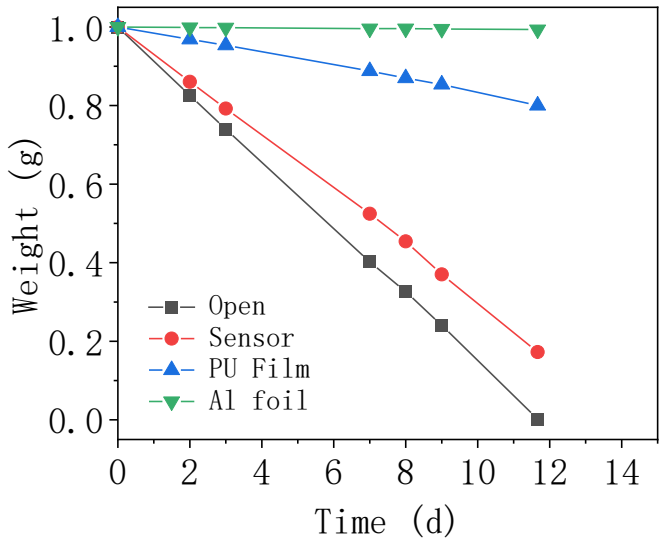

Figure 3.14. Comparison of the water vapor permeability between the sensor and other materials.

3.5 Long-term operation

Figure 3.15 shows the stability of the sensor during storage in bottles with different humidity values for 14 days. Figure 3.16 shows under 35 cycles of repeated changes in relative humidity from 9% to 97%, the sensor impedance showed the same response from approximately 10 MΩ to approximately 1 kΩ.

Therefore, the nanomesh humidity sensor could be used for the continuous measurement of skin humidity for a long time, which is enough for monitoring human activities such as exercise, eating, and grasping objects.

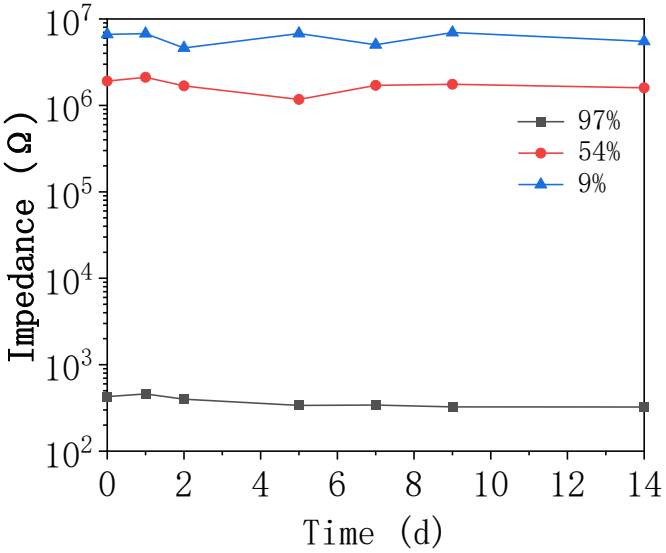

Figure 3.15 Stability of the sensor under different humidity conditions over 14 days.

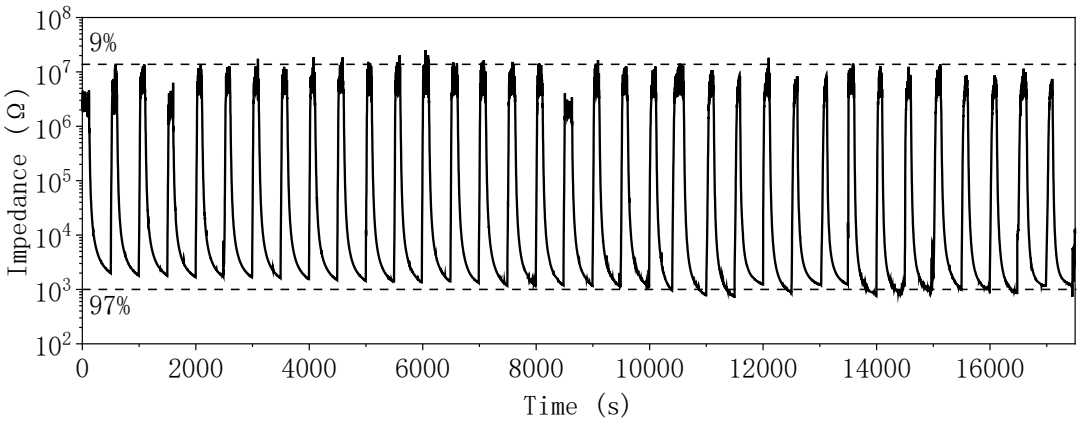

Figure 3.16 Repeatability of the sensor under repeated relative humidity change from 9% to 97%.

Furthermore, the improvements of the sensor by introducing crystallinity-controlled PVA[57] and/or stretchable electrodes[58] would enhance the sensor stability under various environmental conditions and enable a long-term application of the sensors to the skin. It will become an important future direction.

3.6 Influence of sensor structure

Changing the sensor structure resulted in different sensitivities. The change of sensor structure from the current structure to other structures will decrease the sensor

performance, which means the structure plays an important role in the high sensitivity performance of the current sensor. Typically, by replacing the vertical structure of the nanomesh electrodes with the vertical structure, the performance of the sensor dramatically decreased. Also, by replacing the nanomesh-based porous structure with a spin-coated film structure, the sensitivity decreased. This evidence proves that the high sensitivity was highly related to the sandwiched multi-layer nanomesh porous structure.

3.6.1 Vertical structure and lateral structure

When the vertical structure (Figure 3.18a) was changed to a lateral structure (Figure 3.18c), the sensitivity decreased from 640,000% to 1,500% in the 40%–100% RH range. Figure 3.17 shows the structure of the lateral structure. The electrode size was changed to an interdigital shape in lateral structure, with 7 fingers and 0.4 ×12 mm size for each finger. The distance between electrode fingers is 0.4 mm. On the other hand, in the vertical structure, the electrodes have a distance of about 6 μm, which is about 100 times the electrode distance for the vertical structure. Such a huge difference in the electrode distance causes a large impedance and sensitivity difference.

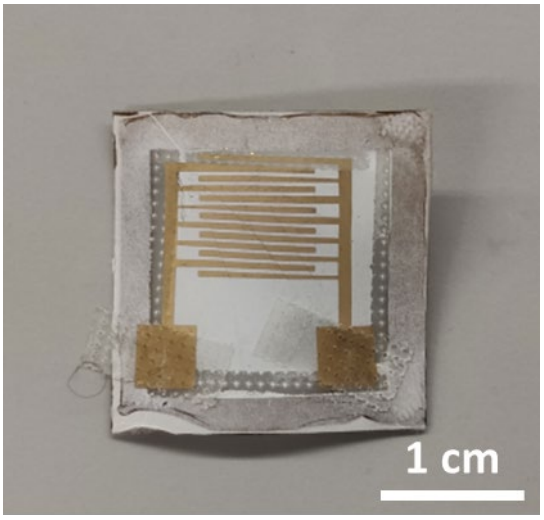

Figure 3.17 The lateral structure of the nanomesh humidity sensor

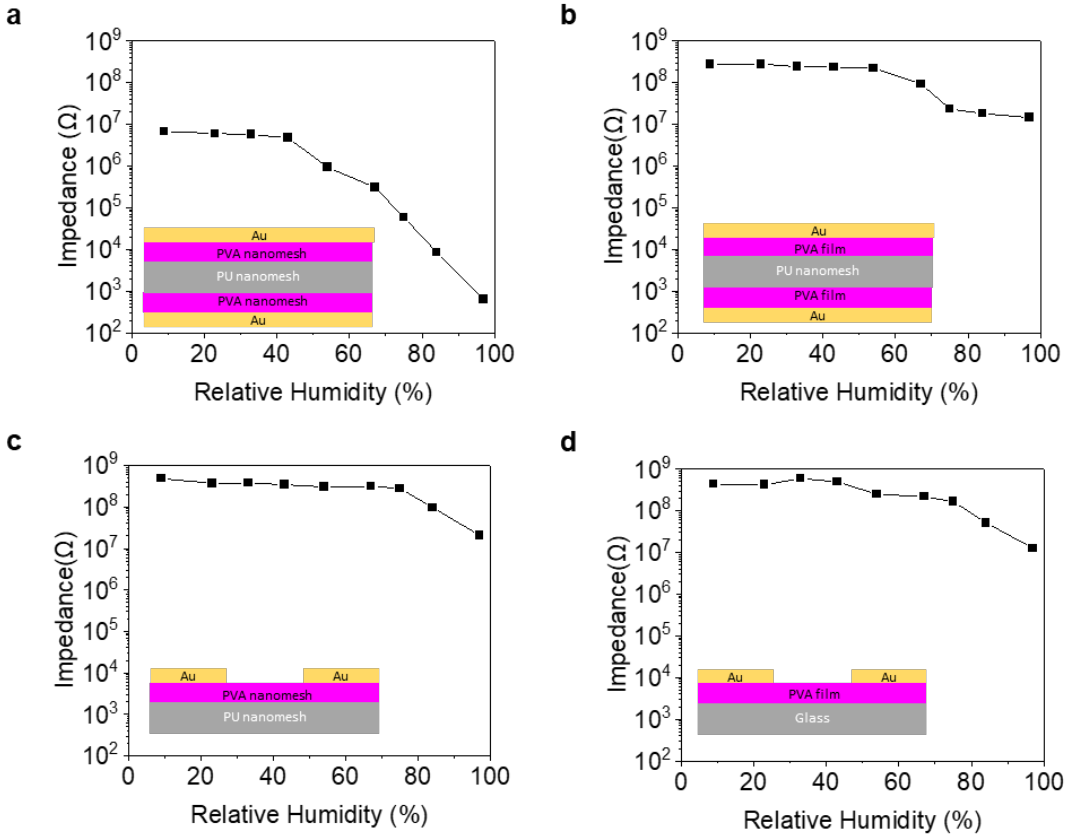

Figure 3.18 The influence of the sensor structure on the sensor's response to humidity change.

3.6.2 Vertical structure and lateral structure

When the PVA nanomesh (Figure 3.18a) was replaced by a spin-coated PVA film (Figure 3.18b), the sensitivity decreased from 640,000% to 1,600% in the 40%–100% RH range. Figure 3.18 shows the fabrication process of the film-based humidity sensor. The difference between the porous nanomesh structure and the continuous film structure results in the different abilities of PVA to penetrate into the PU nanomesh. After applying ethanol and partially dissolving PVA, the nanomesh structure enables PVA to penetrate into PU nanomesh and form an electrically conductive path. But for continuous PVA film, little PVA could penetrate into the PU layer, which leads to a high impedance and limited sensitivity.

4. Mechanical and environmental durability

4.1 Sensor performance under mechanical deformations

The pursuit of mechanically flexible electronic devices started more than 20 years ago, by forming polymer-based transistors on bendable sheets of plastic[59, 60]. Advances in micro and nanopatterning methods[61] and organic semiconductor materials[62] push the development of this field to prosper. In recent years the development of graphene[63], carbon nanotubes[64], and nanowires[65] increased the possibilities of utilizing different materials in intrinsic bendable and stretchable electronics.

Recently, the development of electrospinning nanomesh structures attracts attention in many fields[18, 66]. The developed nanomesh devices show ultra softness with Young's modulus of 274 kPa. With the developed soft devices, a conformable attachment of the sensor with the cardiomyocyte sheets shows precise monitoring of the heart's dynamic motions.

In this work, the nanomesh substrate with both a hydrophobic middle layer and the hydrophilic humidity-sensitive layer was developed. The nanomesh structure makes the sensor flexible and conformal to concave and convex surfaces. The results sensor shows good mechanical durability and flexibility under mechanical deformations such as pressing and bending.

4.1.1 Pressing

Figure 4.1 shows the effects of pressing and bending on the sensor. A pressure of up to 10.2 kPa was applied to the sensor. At 60% RH, the sensor impedance changed from 2.41 MΩ (no pressing) to 0.760 MΩ (10.2 kPa). Such a result shows that the sensor is able to work under pressing with the commonly seen touching situations.

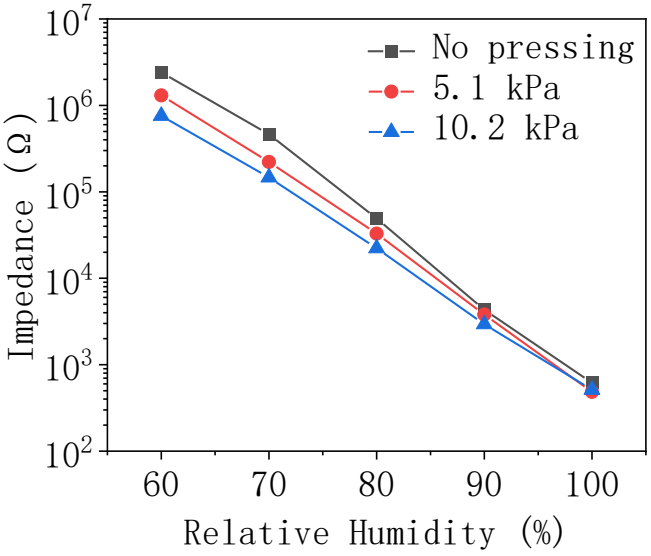

Figure. 4.1 The sensor's sensitivity under different pressure

Figure 4.2 shows the sensor operation under different pressures. The sensor exhibits clear change when the environmental humidity changes. The sensitivity under high pressure exhibited a slow response because the pressing objects covered the sensor surface.

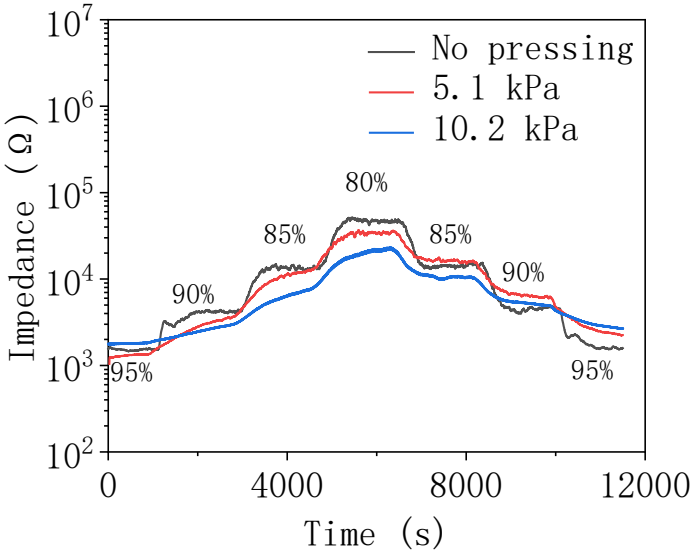

Figure 4.2 Response of the sensor to step humidity changes under different pressing pressures.

4.1.2 Bending

Attaching the sensor to bending surfaces with bending radii of 1.1 and 1.9 cm (Figure 4.3) had an only small influence on the sensor performance. Because of its capability for continuous measurement under bending, the sensor can be attached to curved surfaces, such as skin, for long periods. The sensor can maintain its working function under mechanical influences, which is because of the flexibility property of the nanomesh structure. Figure 4.4 shows the sensitivity under different bending radii.

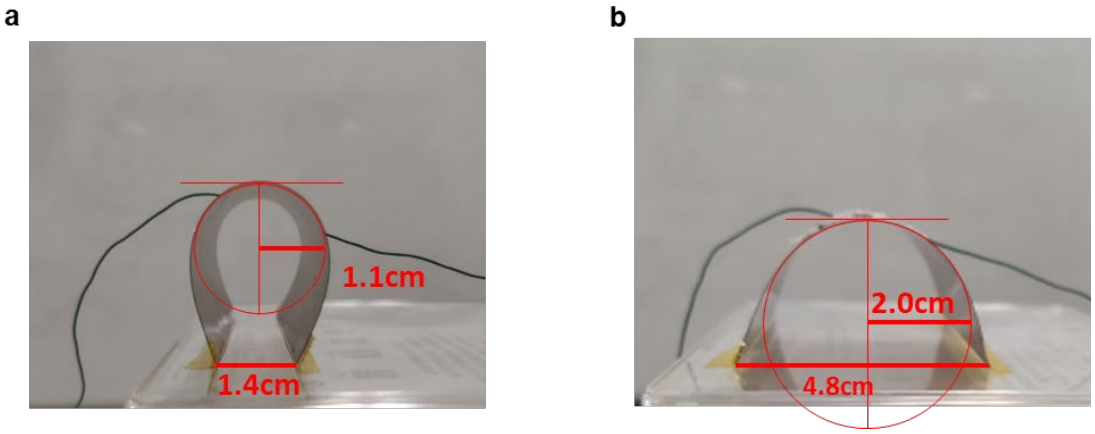

Figure 4.3 Photos of the bending test experiment setup.

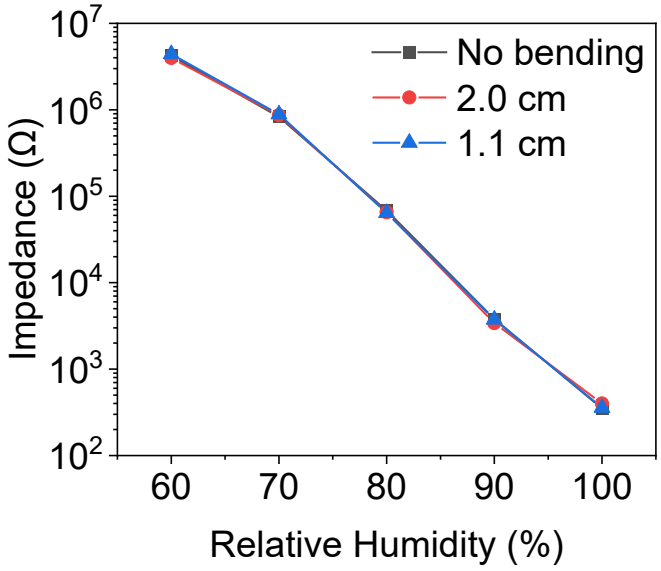

Figure 4.4 Sensitivity of the sensor under different bending radii

Figure 4.5 shows the continuous measurement under humidity changing. A strain within

20% induces a resistance change of only 28% for the nanomesh electrodes[67], and a pressure of 30 kPa only changes the capacitance of the nanomesh sandwich structure by 30%[66]. However, the impedance of the humidity sensor exhibited a large relative change of 640,000% in the range of 40%–100% RH. These results demonstrate that the nanomesh humidity sensor can be operated under mechanical influence.

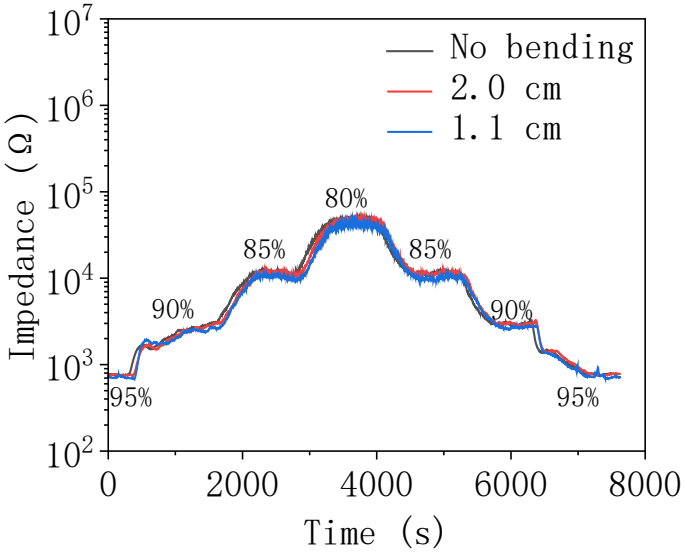

Figure 4.5 Response of the sensor to step humidity changes under different bending radii

4.2 Sensor performance under friction

The nanomesh sensors also exhibit durability against friction. According to previous research, the sensor still remains its sensing function under even rubbing friction with vertical pressure of more than 100 kPa. To evaluate the mechanical durability of the sensor under friction, the following experiments are designed. A spherical polyurethane (PU) ball of 3-mm diameter was used for attachment to the sensor surface. The experiments were done by repeatedly rubbing the surface of the sensor with this polyurethane ball. Figure 4.6 shows the experimental setup of the friction test. The friction force could be changed by the loading weight on the top of the rubbing ball.

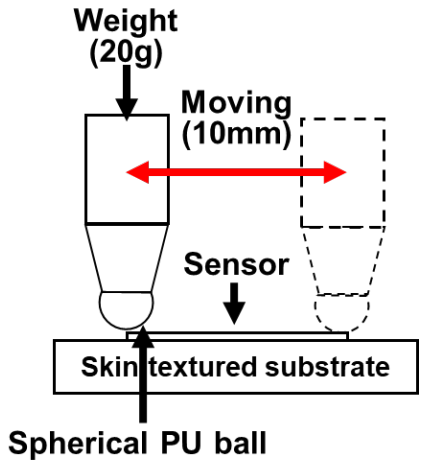

Figure 4.6 Experiment setup for the friction test

4.2.1 Mechanical response

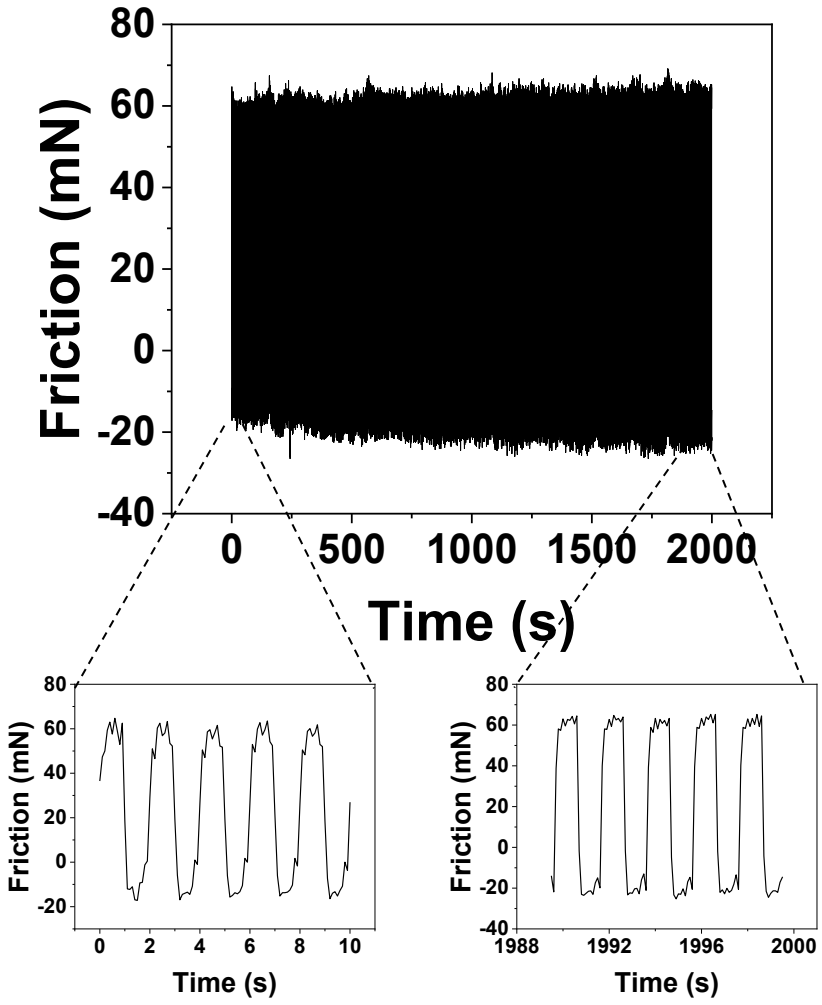

Figure 4.7 Sensor's mechanical response to the friction force

In this work, an external force of 20g weight and a pressure of up to 160 kPa was added to the sensor. The moving speed of the polyurethane ball was set as 20 mm/s. The change in the measured mechanical force on the tip of the contact ball shows the repeated friction force added to the sensor. Figure 4.7 shows the result of the mechanical response from the measurement.

As shown in Figure 4.7, a friction force of positive 60 mN to negative 20 mN was added to the sensor. It shows respectively forward and backward friction. The rubbing of the sensor continued a total of 1000 repeating times. The mechanical force at the beginning of the rubbing and the ending of the rubbing shows almost no difference, which reflects the good mechanical durability of the nanomesh-based humidity sensor.

4.2.2 Electrical response

The performance of the humidity sensor was measured by the electrical impedance of the sensor. The electrical performance of the sensor shows how well the sensor can keep its function ability under friction.

According to reference[66], the functionality of the Au nanomesh electrode was measured after the application of friction. The conductance of the nanomesh electrode with and without the passivation layer was measured. The result shows the conductance of the nanomesh electrode without the passivation layer showing a degradation. When increasing the loaded weight from 10 to 70 g, the conductance finally decreased to less than 1.05×10^{-4}S. However, under the situation of Parylene coated encapsulation, the electrode shows less degradation than the sensor with encapsulation. The result shows that encapsulation can effectively decrease the effect of rubbing.

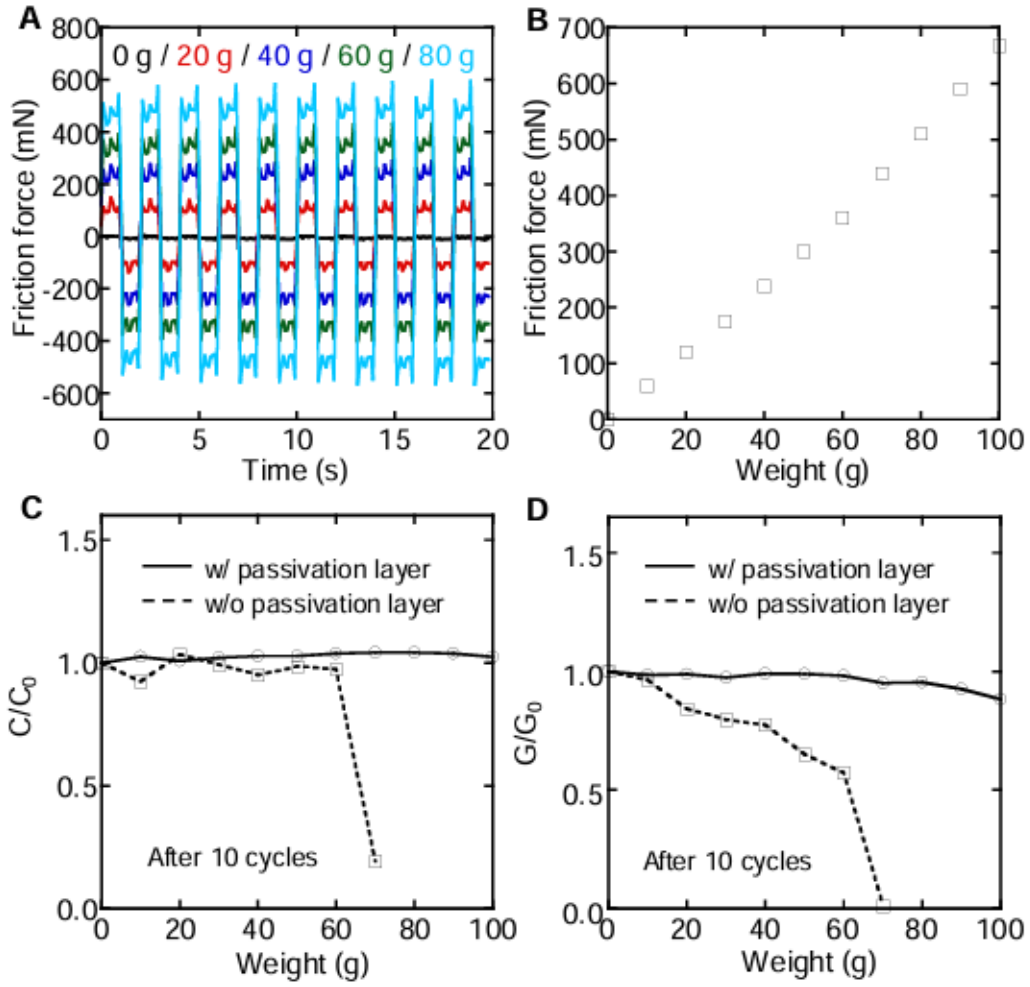

Figure 4.8 Friction experiments with various weights. A-B. Friction forces with different weights. C. Normalized capacitance after friction test. D. Normalized conductance of Au nanomesh electrode after friction test. Copied from reference[66]

Figure 4.9 shows the electrical performance of the nanomesh humidity sensor. Under the repeated friction of a total of 1000 times, the electrical performance of the humidity sensor shows no degradation. The result shows the possibility of the sensor to be used under common situations such as human finger frictions.

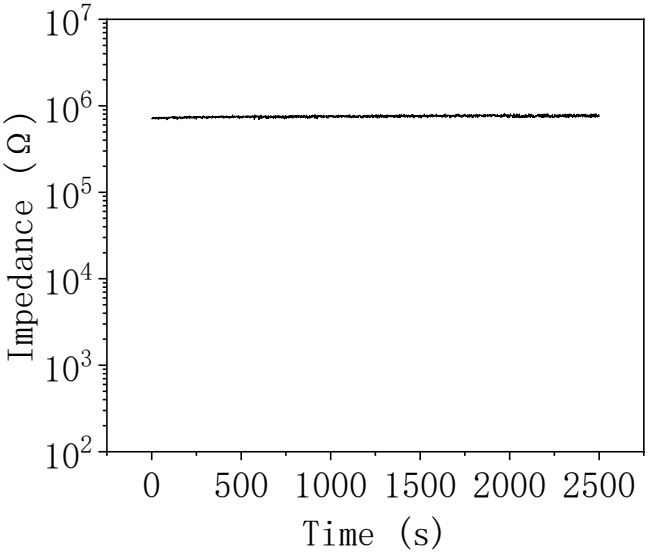

Figure 4.9 Impedance of nanomesh humidity sensor under friction test

4.3 Sensor performance under stretching

Soft electronics have a target to realize the stretchability for applications of on-skin devices. Usually, stretchable electronics are achieved by two kinds of strategies, one is by utilizing the intrinsically stretchable materials which can exhibit stretchability, and another strategy is to use conventional materials with new specially designed structures which show stretchability.

In this work, the stretchability of the nanomesh structure was utilized. Previous research already shows that the nanomeshes exhibit much larger stretchability and much larger gauge factor than traditional thin films. The nanomeshes that have a crossing fiber structure are able to release the strains by the deformations of the structure itself. As a result, under the same stretching strain, the nanomesh sensors will exhibit better performance than the film-like structure.

4.3.1 Mechanical response

The measurement setup for the mechanical response test was shown in Figure 4.10. The sensors were attached vertically to the clamps of the high-precision tensile tester (AG-X, Shimadzu). Then the stretching length and the mechanical force were measured at

the same time.

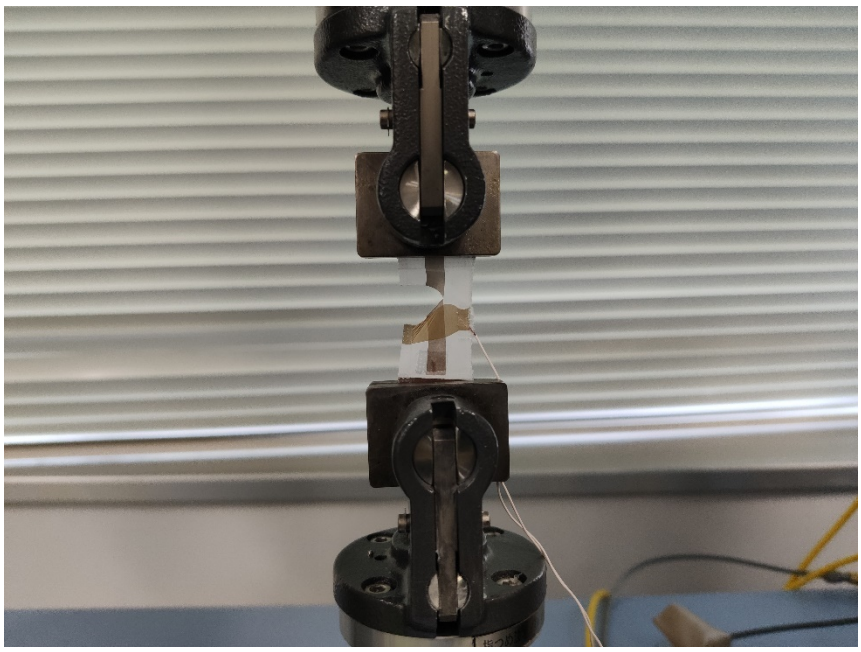

Figure 4.10 Measurement setup of the force stroke curve

The measured results are as shown in the following figure 4.11. The curve has two dramatic fallen of force. The reason for the force drop is the tensile distribution in the sensor is not uniform. Which causes the sensor to first get broken under the only polymer mesh parts (without Au coating), under a stroke of 9 mm, as shown in Figure 4.10. Then the sensor exhibits another broken under the stroke near 12 mm, and the broken happens at the other side of the nanomesh sensor. The middle parts with Au coating maintain the strongest mechanical durability and break at last until 13 mm.

The humidity sensor exhibits the largest stretching length of 8mm (40% of the total length of the sensor) without breaking. This allows the sensor to work under stretching in common skin-attachable situations.

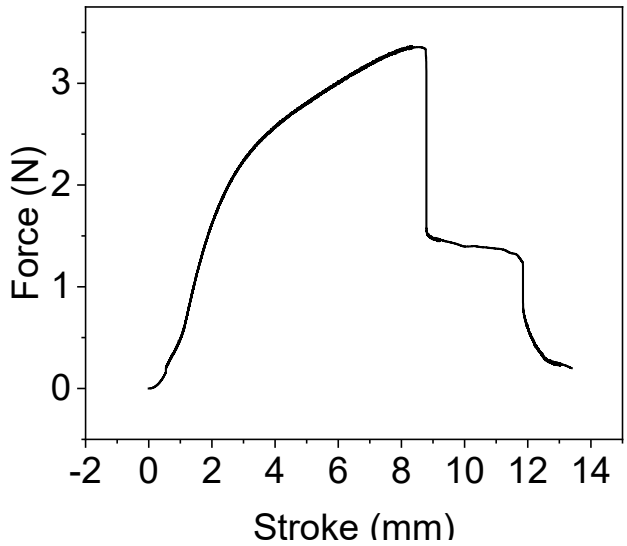

Figure 4.11 The force stroke curve of the humidity sensor

4.3.2 Electrical response

The electrical response of the sensor was measured by the impedance change of the humidity sensor under stretching. Also, the sensor's response to humidity change was measured by a human finger approach before and after the stretching test.

In this work, the electrical response was measured by the following methods. First, the sensor was attached to a stretcher (Thorlabs APT user) after removing the PI frame. The repeated stretching/ releasing cycles of 20% strain (0.4 cm) were applied to the sensor. First, the sensor's response to the human finger humidity was measured, and the impedance of the sensor decreased from 10^6 Ω to 10^4 Ω. Then 50 cycles of stretching were added to the sensor. After that, the sensor's response to the human finger humidity was measured again and the impedance change are in the same range as before. Next, another 50 cycles of stretching were added to the sensor, and the impedance change by the human finger humidity was still the same value as before. The measurement of the electrical performance change shows the sensor's durability under repeating stretching tests.

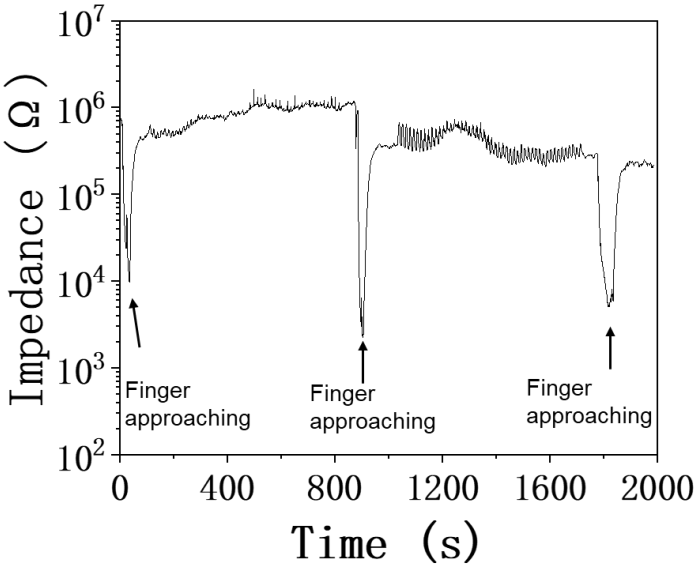

Figure 4.12 The impedance changes of the nanomesh humidity under repeated stretching/releasing test and the human finger approaching

4.4 Sensor performance under temperature change

In this work, the effect of the temperature on the sensor performance was also evaluated. The influence of the temperature is important since temperature variation such as skin temperature change, and environmental temperature change will influence the sensor performance. In an ideal case, a temperature-insensitive sensor should be developed. However, usually, the humidity sensor performance will be influenced by temperature. In such a case, measurement of the temperature influence on the sensor and the simultaneous measurement of the temperature together with the humidity is very important. Based on the data on the temperature influence, the resulted data can be calibrated.

Figure 4.13 shows the sensor's response to 60-100% RH under the temperatures of 25℃, 30℃, 35℃, and 40℃. When the temperature increases, the impedance of the sensor shows decreasing. One of the main reasons for this result is: That under the same relative humidity, when temperature varies, the absolute humidity of the environment is changing, and the water molecules' contents are increasing, which leads to more water molecules being absorbed in the sensor's nanomesh structure, decrease the impedance

of the sensor.

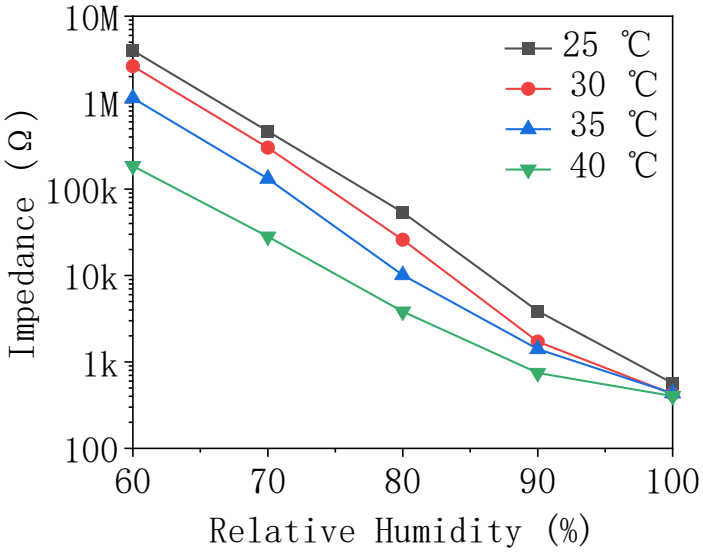

Figure 4.13 Sensor's response to the relative humidity under different temperatures

Then, the relative humidity was changed into the absolute humidity (which was shown as water weight per unit volume), and the figure was plotted again to show the influence of the absolute humidity, as shown in Figure 4.14.

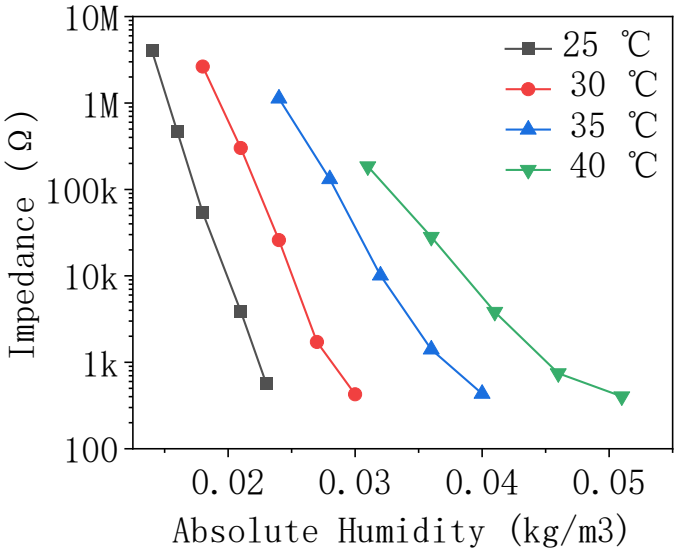

Figure 4.14 Sensor's response to the absolute humidity under different temperatures

Here, under the same value of absolute humidity, the increase in the temperature leads

to the increase of impedance. The reason is possibly due to the condensation of the water vapor will decrease.

At lower temperatures, the sensor had a higher sensitivity. When the temperature increases and relative humidity maintains, the absolute humidity will increase, and more water molecules lead to a lower impedance, thus the overall impedance changing is low and sensitivity is decreased.

4.5 Sensor performance under object approaching

The sensor's performance under the approaching of different objects was also tested in this study. The conductor, non-conductor, and non-conductor wrapped with napkins were used for experiments. The objective of this experiment is to investigate if the effects such as electromagnetic field coupling or remaining charges on materials have an influence on the humidity sensing properties.

The result of the object approach is shown in Figure 4.15. Only the non-conductor wrapped with a wet napkin will rise impedance change on the sensor. The approaching of objects to the sensor itself has no influence on the sensor property.

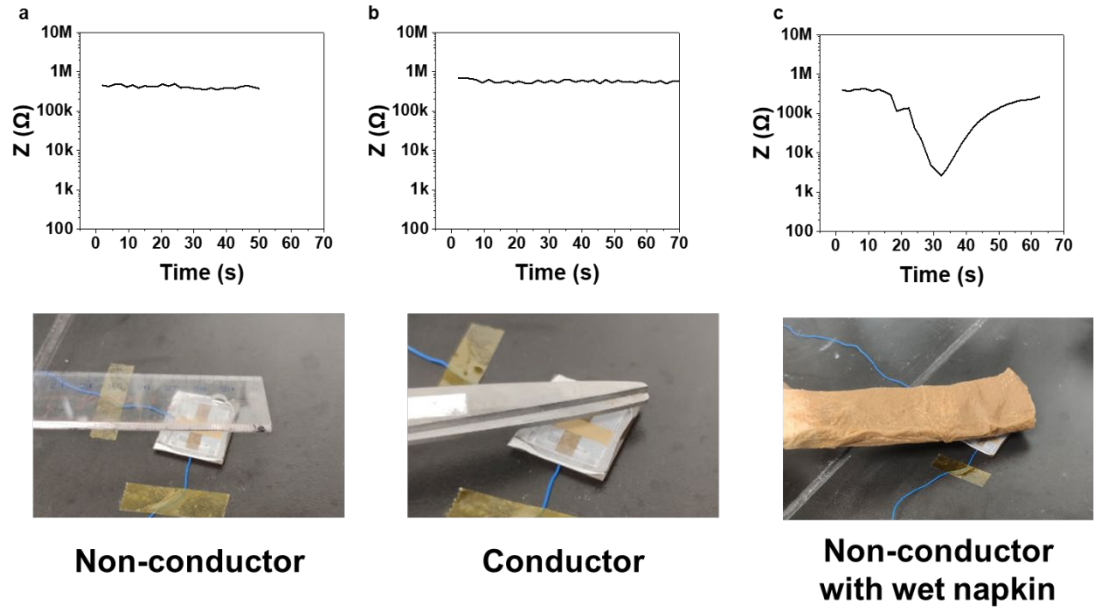

Figure 4.15 The influence of the object approaching on the sensor's response to humidity

5. Circuit model and impedance analysis

5.1 Complex impedance analysis

In the analysis of the humidity sensing mechanisms, the method of complex impedance spectroscopy analysis was usually performed. Basically, the complex impedance analysis is based on the phasance concept[68, 69].

For an electrical device, an alternating voltage is applied to the whole device and is expressed by a function of time, V(t), causing a response current, I(t), to flow in the electrical device. The relationship between the voltage and the current can be expressed by the impedance(Z)., which is expressed by $Z = \frac{V}{I}$. The impedance is an argument with both amplitude and phase, shown as $Z = P_{\varphi}(i\omega)^{\nu}$, here constant P_{φ} represents the amplitude of the impedance and ν represents the phase of the impedance. The consideration of resistance, capacitance, and inductance as boundary cases of phasance, leads to a more general approach in mathematical treatments, which will also be introduced later.

The Impedance can be regarded as a value to describe the property of a system by the ratio between the emitted signal (Current) and the input signal (Voltage). A common method to measure the electrical property is by measuring the current and the voltage under various input frequencies f or $\omega = 2\pi f$, and then analyzing the impedances under different frequencies. The complex impedance is expressed by $Z = Z' + iZ^{"}$, where i is the imaginary unit and Z' is the real part of impedance and $Z^{"}$ is the imaginary part of the impedance. The admittance, $Y(\omega)$ is defined as the reciprocal of the impedance Z, $Y(\omega) = \frac{1}{Z}$.

In the research related to dielectrics, the experimental data are usually represented by the following equation[69], which is called the complex permittivity:

$$\varepsilon = \varepsilon_p + \frac{\varepsilon_s}{1+(i\omega\tau)^{1-\alpha}} \tag{17}$$

When the complex permittivity is semi-circles that the centers of which are depressed

below the real axis, this behavior is referred to as non-Debye. In the field of ionic conductors, it has long been recognized that many complex impedance loci result in well-defined semi-circles. An empirical formula was usually used as a description of the experimental results.

$$Z = R_s + \frac{R_p}{1+(i\omega\tau_0)^{1-\alpha}} \tag{18}$$

In electrical circuits, the basic components of resistance, inductance and capacitance help to build the model of the whole circuit. The following table concludes the general rules for the three basic components and the difference with the phasance. Then the need for introducing the phasance as a component was concluded.

	Basic Laws	**Degree of derivation**	**Magnitude coefficient**	**Phase displacement**	**Impedance**
Inductance	$V = L\frac{dI}{dt}$	$\nu = +1$	$P_\varphi = L$	$\varphi = +\frac{\pi}{2}$	$Z = Li\omega$
Resistance	$V = RI$	$\nu = 0$	$P_\varphi = R$	$\varphi = 0$	$Z = R$
Capacitance	$V = \frac{1}{C}\int Idt$	$\nu = -1$	$P_\varphi = \frac{1}{C}$	$\varphi = -\frac{\pi}{2}$	$Z = \frac{1}{i\omega C}$
Phasance	$V = P_\varphi \frac{d^\nu I}{dt^\nu}$	ν	P_φ	$\varphi = \frac{\pi\nu}{2}$	$Z = P_\varphi (i\omega)^{\frac{2\varphi}{\pi}}$

5.2 Circuit model

In this work, the following circuit model was proposed. In the equivalent circuit, R1 and C1 correspond to the electrical properties of the PVA–PVA interaction, R2, and C2 correspond to the electrical properties of the PVA–Au interface and R3 represents the bulk resistance of the connecting wire and electrodes.

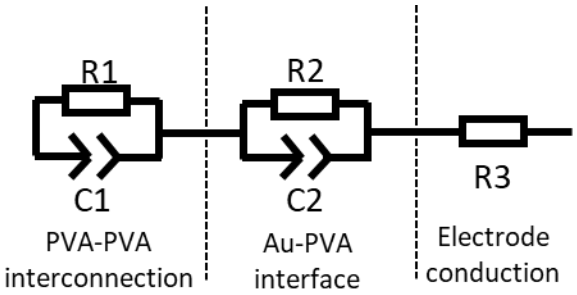

Figure 5.1 Equivalent circuit of the sensor. R1, R2, and R3 are resistors, and C1 and C2 are CPEs.

The model was built based on the impedance angle results. Two semicircles existed in the impedance angle versus frequency curves, which correspond to a polarization mechanism[70, 71]. This polarization phenomenon can be described by an equivalent circuit of the parallel connected resistor and capacitor [72, 73]. As explained above, for the porous materials like the nanomesh structure in this research, the non-Debye behavior exists. The capacitance behavior is not an ideal component and the derivation degree is not fixed to -1. In such a case, the constant phase element is suitable for describing the electrical behavior of the sensor.

In the equivalent circuit, R1 and C1 correspond to the electrical properties of the PVA–PVA interaction, R2, and C2 correspond to the electrical properties of the PVA–Au interface and R3 represents the bulk resistance of the connecting wire and electrodes.

An impedance analysis based on a proposed circuit model is constructed. The impedance of the equivalent circuit can be expressed as follows:

$$Z = \frac{1}{\frac{1}{R_1}+(i\omega)^{n_1}C_1} + \frac{1}{\frac{1}{R_2}+(i\omega)^{n_2}C_2} + R_3 \tag{19}$$

And the impedance angle φ which is expressed by the complex number argument can be calculated to the following equation.

$$\varphi = arctan\left[\frac{\omega C_1 R_1^2(1+\omega^2 C_2^2 R_2^2)+\omega C_2 R_2^2(1+\omega^2 C_1^2 R_1^2)}{R_1(1+\omega^2 C_2^2 R_2^2)+R_2(1+\omega^2 C_1^2 R_1^2)+R_3(1+\omega^2 C_1^2 R_1^2)(1+\omega^2 C_2^2 R_2^2)}\right] \tag{20}$$

When the parameters R_1 to R_3 and C_1 to C_2 are fixed as constants, the circuit model is determined. When calculating the impedance of this circuit under different frequencies

ω, the impedance Z and the angle φ are changed due to ω changing.

Based on this circuit model. We conducted a curve fitting based on the experimental data of impedance Z and the angle φ. R_1 to R_3 and C_1 to C_2 are parameters to be determined. By doing the curve fitting under different relative humidities of 9%-97%, R1-3 and C1-2 are determined. The resulted bode diagram was shown in Figure 5.5.

5.3 Impedance fitting results

5.3.1 Bode diagram

Bode diagrams are figures that show the frequency responses of a system. Usually, the magnitude (amplitude) and the phase (angle) are shown in different graphs, under a logarithmic frequency scale along the x-axis. 0-frequency (DC response) will correspond to negative infinity on the x-axis and not be shown on the plots[74].

For example, consider the circuit, which is composed of a paralleled connected resistor and capacitor and a following series connected resistor. The circuit can be shown as the following Figure.

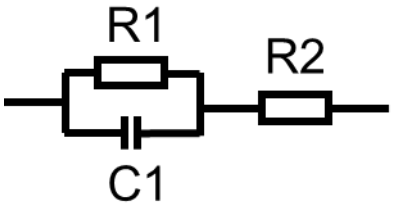

Figure 5.2 The example equivalent circuit

The impedance of the circuit can be shown as the following equation:

$$Z(\omega) = R_2 + \frac{R_1}{1+i\omega C_1 R_1} \tag{21}$$

Here, R_1 and R_2 are the resistance value of the resistors R_1 and R_2, respectively; C_1 is the capacitance value of the capacitor, $\omega = 2\pi f$ which is the angular frequency, and i is the imaginary number unit.

Then, the impedance value was calculated under different frequencies and the results of impedance amplitude and the impedance angle were shown in Figure 5.3.

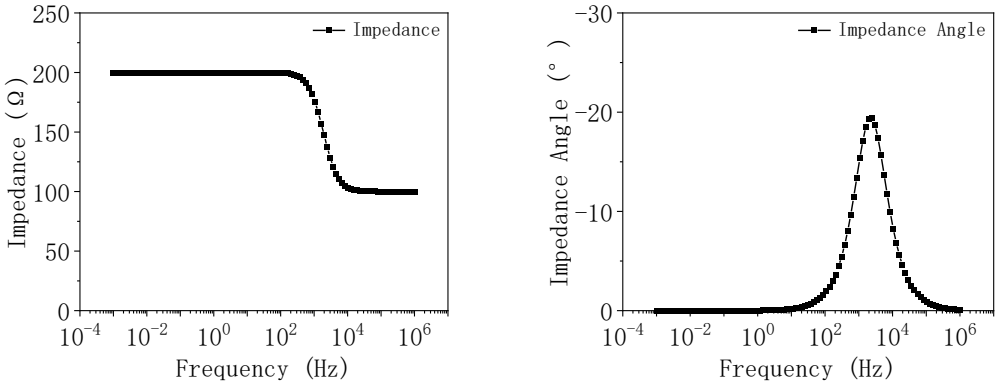

Figure 5.3 The Bode diagram of the example equivalent circuit.

As shown in the figures, the impedance magnitude has a decrease in the frequency of 2000 Hz. At the same frequency, the impedance angle will show a peak. This kind of phenomenon shows how the peak shape generates in the equivalent circuit. In the curve fitting of the equivalent circuit, the parallel connected resistor and capacitance can be utilized to simulate a peak shape in the bode diagram.

Figure 5.4 and Figure 5.5 show the impedance angle of the sensor impedance under three different humidities. Figure 5.6 shows the details of the impedance angle curve. The impedance angle changing under different RHs reveals further information about humidity sensing. At 9% RH, the sensor had an impedance angle near -90°. At 54% RH, the impedance angle was between -90° and 0°, and at 84% RH, the impedance angle value decreases a lot compared to the low humidity situations.

The similar impedance angle and impedance Nyquist diagram of the experimental and equivalent circuit fitting results signified the rationality of the equivalent circuit (Figure 5.5).

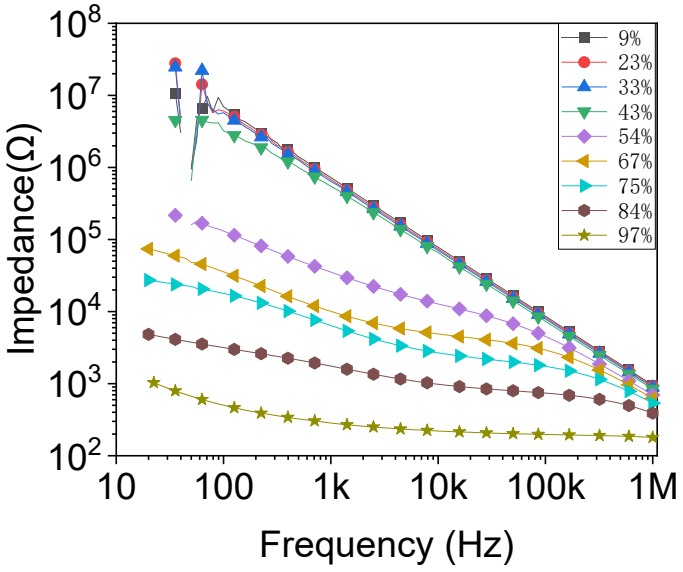

Figure 5.4 The impedance amplitude of the sensor under different frequencies

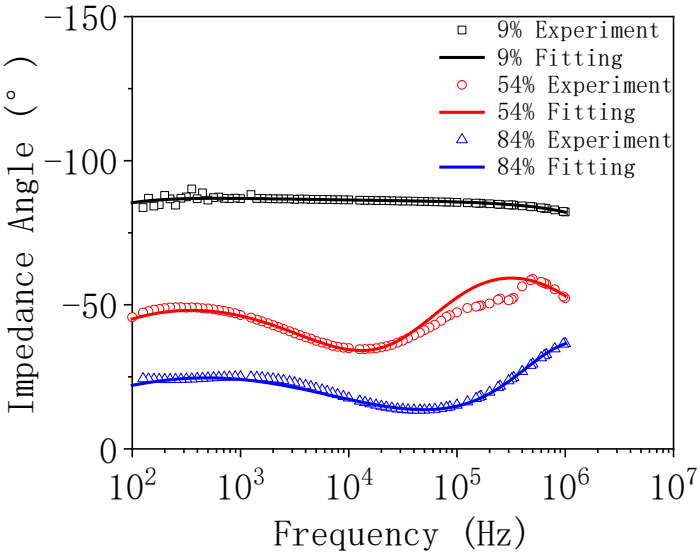

Figure 5.5 The impedance angle of the sensor under different humidities

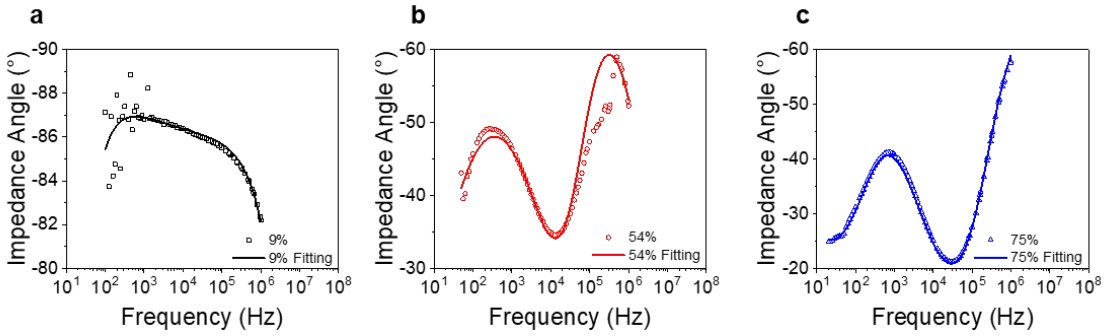

Figure 5.6 Experimental and fitting results of the sensor impedance angle at different humidity levels, with an enlarged scale.

In the low humidity range (9%–43%), few water molecules were absorbed due to the material properties, the resistance decreased owing to the increase in the conductivity, and the capacitance increased owing to the increase in the dielectric constant. In the high humidity range (43%–97%), more water molecules would be absorbed and condensed, which leads to a significant increase in resistance and decrease in capacitance, resulting in a significant decrease in impedance and then increased sensitivity[75, 76].

5.3.2 Nyquist diagram

The Nyquist diagram[77] is one kind of graph in which every point represents the magnitude of the open-loop frequency response at a particular frequency. In the field of electrochemical measurement, the Nyquist diagram is usually used for visualizing the impedance spectrum[78]. By plotting the real part of the impedance on the x-axis and the imagined part on the y-axis, an informative overview of the impedance and distribution of different components can be shown inside the device under test.

There is one shortcoming of Nyquist plots, that is the specific frequency for each data point is missing. Usually, the low-frequency data points will have a larger impedance value, but it is not true for all the circuits.

The different kinds of components will generate different shapes of curves in the Nyquist diagrams. For example, for the equivalent circuit model which was already shown in Figure 5.2. The Nyquist diagram of it can be shown in Figure 5.7.

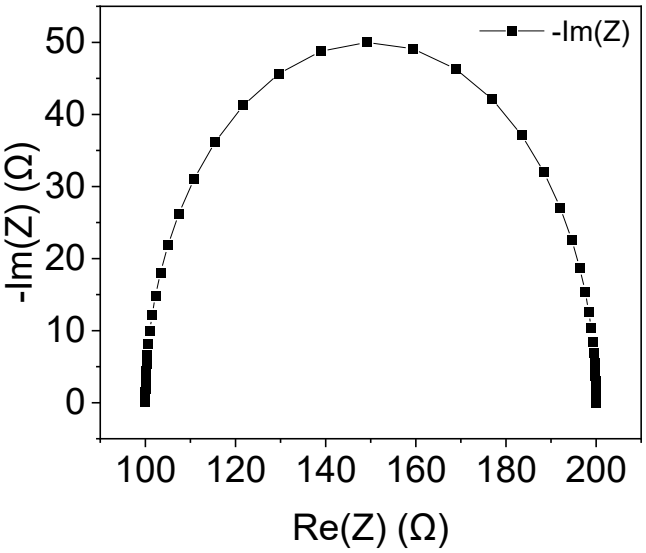

Figure 5.7 The Nyquist diagram of the sample circuit.

As shown in the figure, the most distinctive feature of the curve is the near semi-circle shape of the circuit. The parallel connected resistor and capacitance can be utilized to simulate a semicircle shape curve in Nyquist diagram.

Next, the fitted impedance values are also plotted in Nyquist plots, as shown in Figure 5.8, Figure 5.9 and Figure 5.10. The overlap of the experiment data points and the fitted curve shows the accuracy of the fitting method.

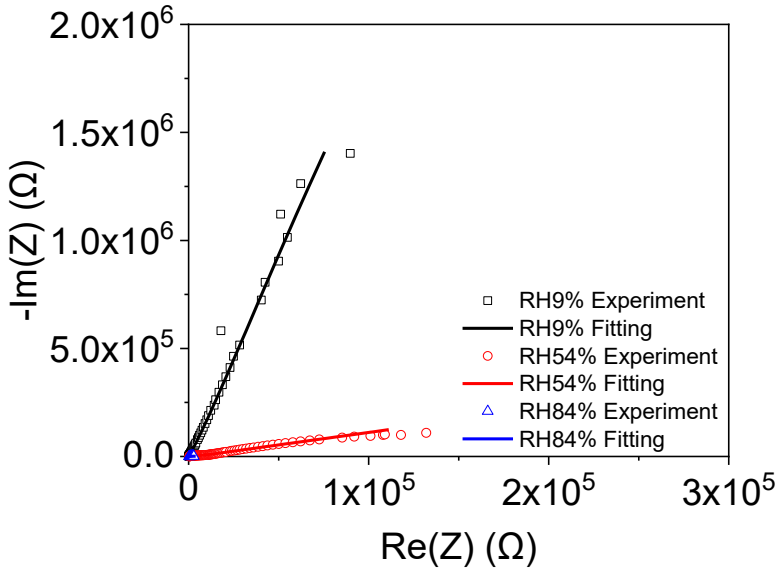

Figure 5.8 The Nyquist plot of the sensor impedance under different frequencies

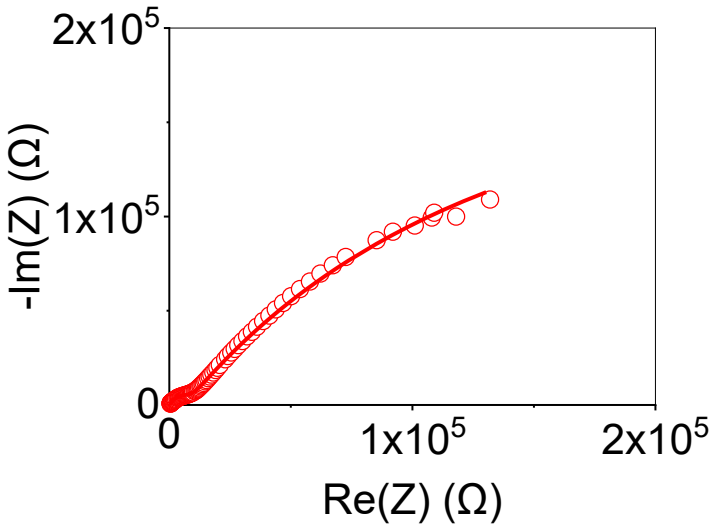

Figure 5.9 The Nyquist plot of the sensor impedance under 54% RH

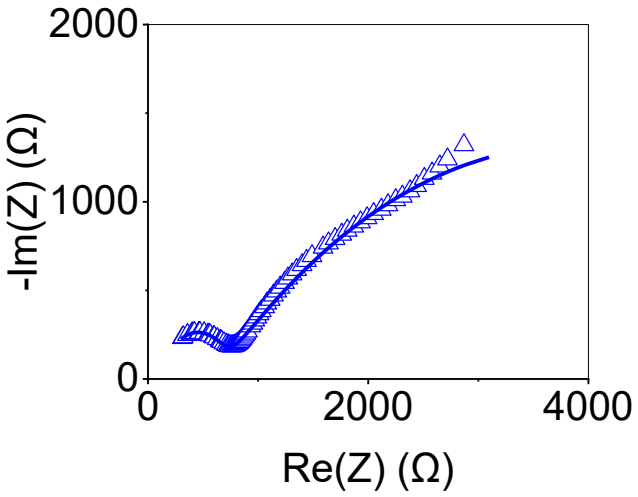

Figure 5.10 The Nyquist plot of the sensor impedance under 84% RH

5.4 Change of capacitor and resistor components

Following the equivalent circuit model building and the complex impedance curve fitting, the resistance values of R_1, R_2 and R_3, and the capacitance values of C_1 and C_2 can be decided as the curve fitting variables.

In this section, the change of the capacitance and resistance under the humidity changes

are concluded, and their relationship with the humidity-sensitive mechanisms is explained.

The overall changing trend of the capacitance and resistance are concluded in Figure 5.11.

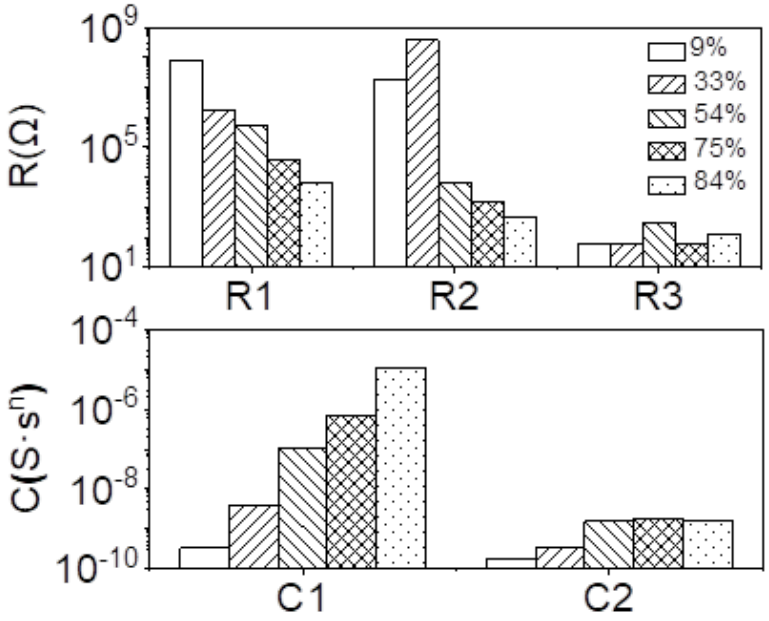

Figure 5.11 The change of resistor and capacitor component values under different humidity levels.

5.4.1 Capacitor

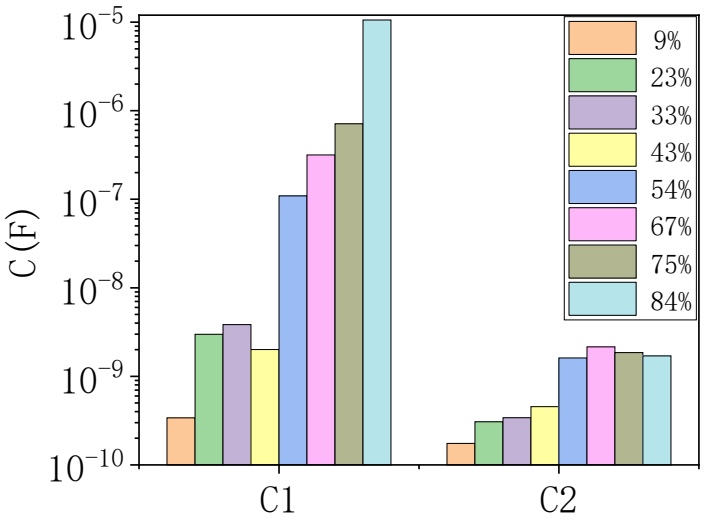

Figure 5.12 The capacitance value changing under different humidities

Figure 5.12 shows the capacitance values from 9% RH to 84% RH. Generally, with the increase in humidity, the capacitance will increase. However, the capacitance value is not always increasing and shows saturation in the high humidity range for C2.

The different behavior can be explained by the mechanism difference between the two components. C_1 represents the capacitor formed between the PVA-PVA interaction, and C_2 represents the capacitor formed at the PVA-Au interface. The PVA-Au interface has a limited space compared with the interaction space of PVA nanomesh scaffolds. The dimensional difference of the two different components is the main reason for the difference in the behavior in the high humidity range, which will also be supported by the results of the resistor fitting results.

5.4.2 Resistor

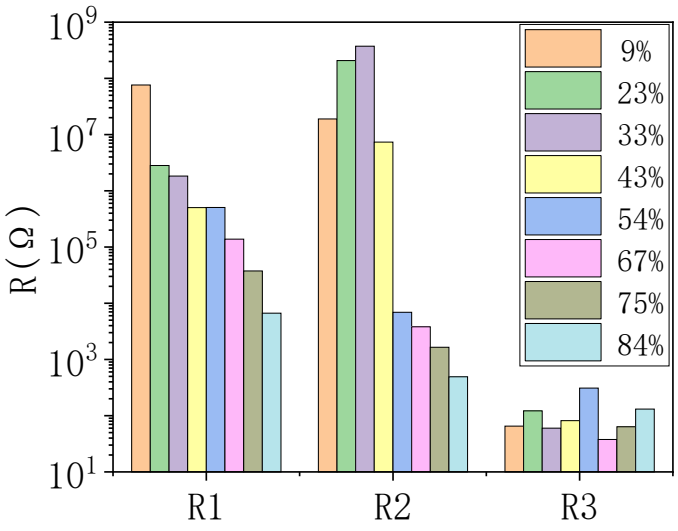

Figure 5.13 The resistance value changing under different humidities

Figure 5.13 shows the resistance values of R1, R2 and R3 from 9% RH to 84% RH. Generally, for R1 and R2, with the increase of the humidity, the resistance values will decrease. However, for the resistor R3, the resistance value will usually keep in a same level. Also, for R1, the overall trend of resistance value is always in decreasing, for R2, the high humidity range also shows the saturation of value decreasing.

The different behavior can be explained by the mechanism difference of the three components. R3 represents the bulky parts of the circuit, including the external connection parts, and the Au conducting parts, which are always constant under humidity change. In Figure 5.12, the value can be concluded to be around several hundred ohms.

R1 and R2 represent different parts of the nanomesh sensor, respectively. R1 represents the resistor between the PVA-PVA interaction. A conductivity will form when the humidity increases, the water molecules will be absorbed in the polymer chains, and the protonation of the molecule will lead to ionic conduction to the sensor. R2 represents the resistor between the PVA-Au interface. The absorption of water facilitates the

increase of the conductivity between the polymer-metal interface. Here, the R2 shows saturation of resistance value under increasing of humidity. The PVA-Au interface has a limited space for water absorption, which leads to a limited absorption ability. Therefore, under the high humidity, the decrease of the resistance become saturated.

6. Human skin humidity measurement

6.1 Distribution of humidity at different positions of human skin

Before using the nanomesh sensor for the measurement of skin humidity, the sensor was used to measure the humidity distribution at different positions of human skin. First, the humidity sensor was approached by a human fingertip at the distance of 10mm, 5mm, and 0mm. At the same time, the environment temperature and humidity were measured. The human finger skin temperature was measured at the same time and the humidity sensor response was recorded by the nanomesh sensor. The environment temperature was maintained at 24.5 ℃, and the environment humidity was from 40-50 % RH. Figure 6.1 shows the measurement of the fingertip.

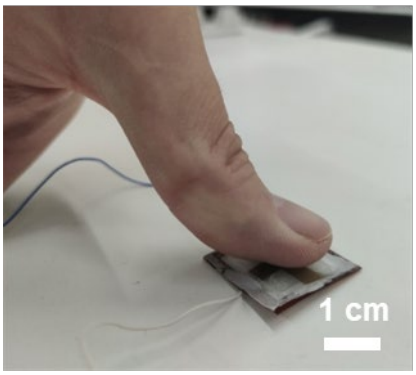

Figure 6.1 Fingertip photo of approaching the nanomesh humidity sensor

The human fingertip usually has a very high humidity level, which makes the sensor have an impedance response same as >90% RH environment. The impedance changes of different approaching distances were recorded in Figure 6.2.

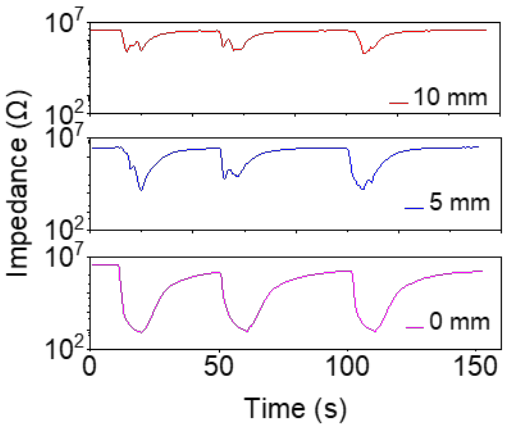

Figure 6.2 Humidity sensor response at different distances from the fingertip surface

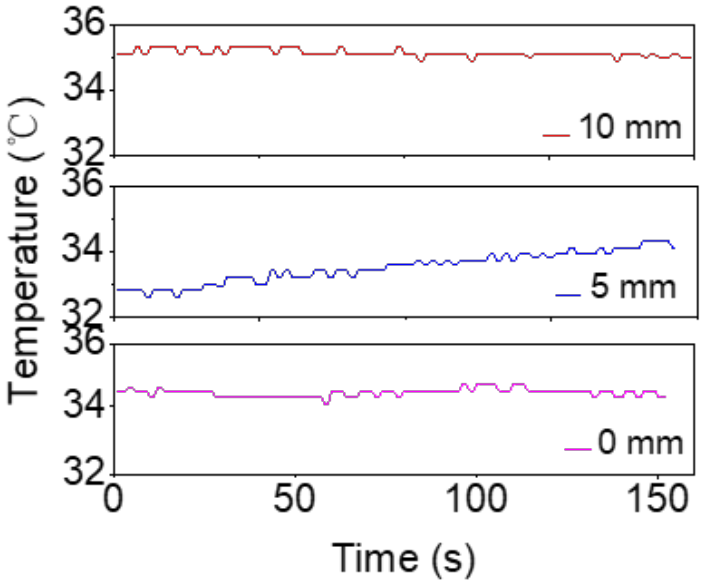

Figure 6.3 The finger skin temperature changes when approaching the nanomesh humidity sensor measured together with Figure 5b. The environment temperature was controlled at 24.5 ℃.

Different distances produce different humidity sensor responses. At 0 mm, the sensor touches the skin. The impedance changes greatly, and it takes a long time for the device to reach equilibrium recovery. The different responses of the sensors confirmed the different humidity levels at different distances from the skin. Temperature changes are recorded in Figure 6.3. During the experiment, the skin temperature of the tested finger was in the range of 33-35°C, with a change of less than 1.6°C. A change of 1.6°C affects

the impedance value by 13%, which is small compared to the change caused by humidity, which is greater than a 1000% change.

After the measurement of the fingertip, the back of the hand and the palm of the hand were measured to detect the humidity. The sensor was attached to the hand as shown in Figures 6.4 and Figure 6.5.

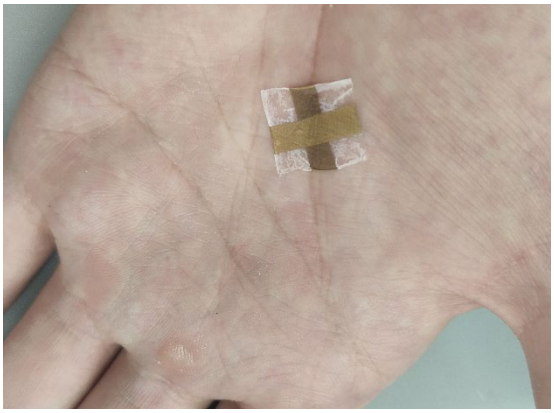

Figure 6.4 The measurement of the humidity at the palm of human hand

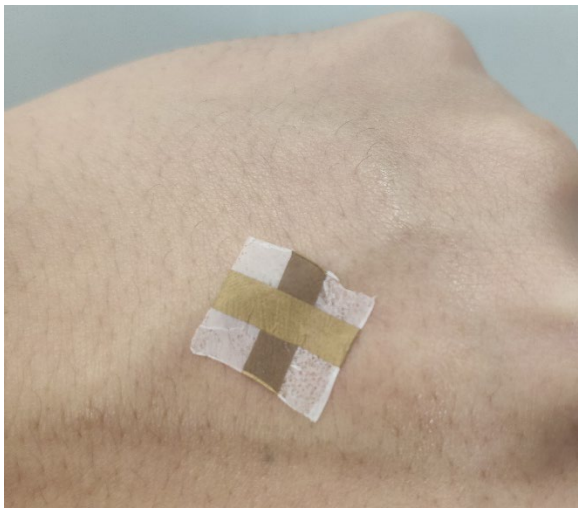

Figure 6.5 The measurement of the humidity at the back of the human hand

A Conformable attachment between the sensor and the skin surface was achieved using an adhesive layer formed from dissolved PVA. In this case, the humidity of the back of the hand and the palm of the hand were measured, as shown in Figure 6.6 and Figure 6.7. When the subjects were at rest, the sweat rate of the back of the hand was lower than that of the palm. There is little moisture on the back of the hand; therefore, the

sensor does not respond to the back of the hand. However, the sensor showed a remarkably large response to palm humidity. These results show that the palm humidity is about 80%.

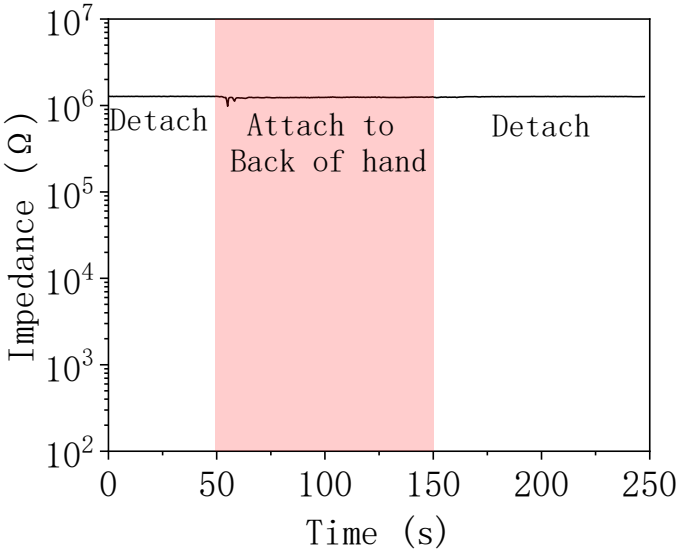

Figure 6.6 Impedance changes of the sensor when it was attached to the back of the hand

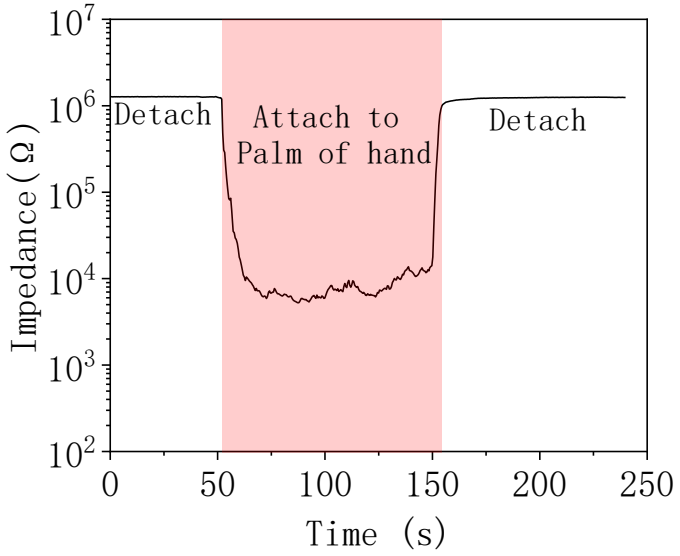

Figure 6.7 Impedance changes of the sensor when it was attached to the palm of the hand

6.2 Continuous measurement of human skin humidity

Continuous measurement of the skin humidity at the back of the hand for an hour was achieved by using a nanomesh humidity sensor. A commercial humidity sensor was attached to the skin surface to validate the nanomesh sensor. The measured impedance values are converted to humidity values by calibration of the skin temperature. Calibration was based on the sensitivity-temperature relationship. During the monitoring period, test subjects were asked to perform two exercises. The result is shown in Figure 6.8. Skin moisture shows the humidity value around 30% at steady state, and during exercise it rapidly increases to around 70%. Skin temperature changes <1.5°C during the measurement; therefore, it has little effect on the humidity measurement (Figure 6.9). The increase in humidity was due to the evaporation of sweat on the surface of the skin. The humidity value declines gradually from the surface to the ambient humidity value. Therefore, the conformal attachment of the sensor to the skin results in more accurate results than conventional humidity sensors. Simultaneous monitoring with a commercial humidity sensor confirmed the accuracy of the nanomesh sensor. Using the proposed sensor, continuous humidity measurement can be achieved without adversely affecting the skin.

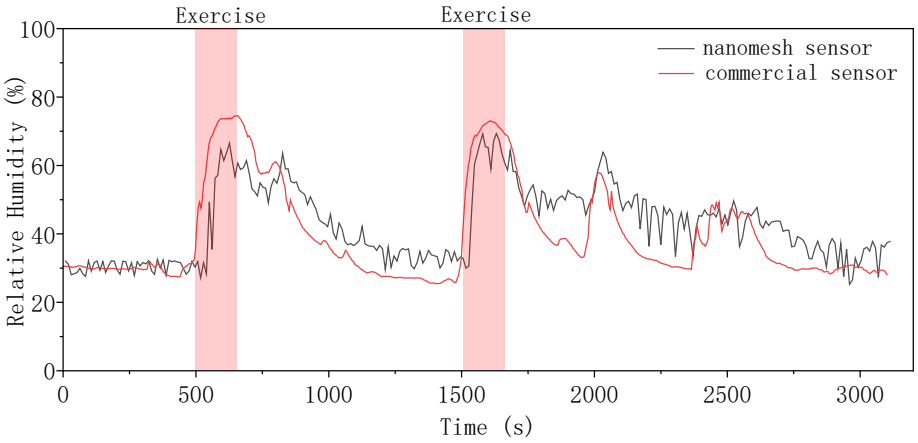

Figure 6.8 Continuous measurement of the skin humidity at the back of the hand together with the commercial humidity sensor. Results were measured at a temperature range of 20 ℃ - 25 ℃ and a frequency of 100 Hz.

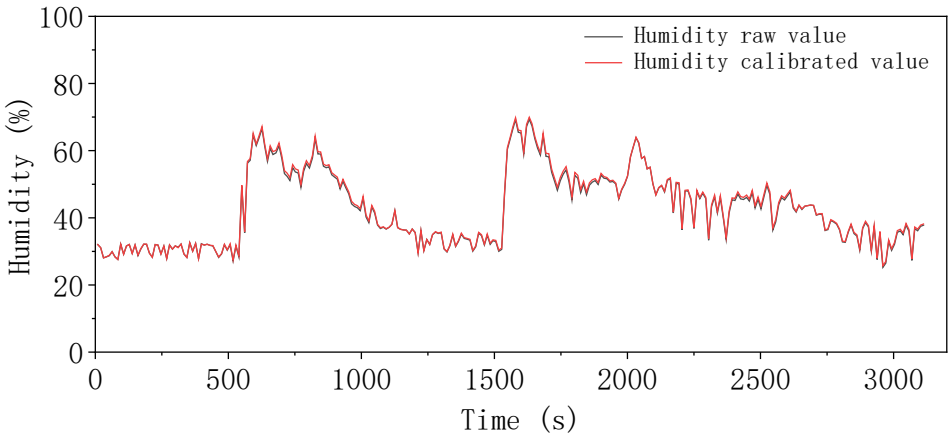

Figure 6.9 Calibration of the temperature influence on the sensor during continuous skin humidity monitoring.

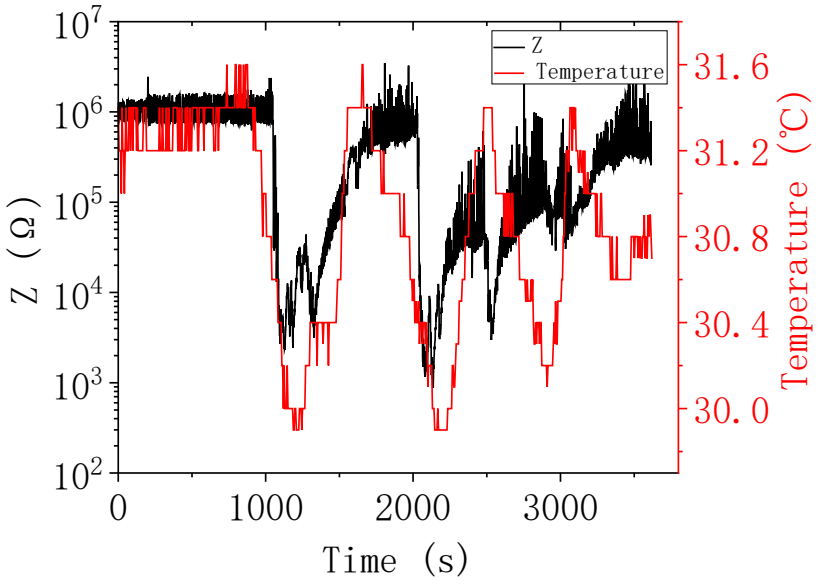

Figure 6.10 Measurement of skin impedance and skin surface temperature at the same time

7. Summary and prospect

7.1 Summary

The gas-permeability is a critical property for wearable devices that are directly in contact with human skin for long-term continuous measurement. Skin attachable humidity sensors measure the sweating and transepidermal water loss, which is related to the water contents. The gas-permeability becomes more important in the sense of accurate measurement. In this study, for the first time, we successfully developed the porous nanomesh structure humidity sensor that has gas-permeability, high sensitivity, and flexibility together. The gas-permeable humidity sensor can eliminate the risk of accumulated moisture between the sensor and skin, rendering the long-term wearing and measurement.

The ultrathin and flexible nanomesh was used for the lamination of the sensor. We explored the process of fabricating the nanomesh sheet and the integration of multiple layers to work as a whole part. The morphology of the nanomesh structure was investigated through SEM images.

Next, the basic performance of the humidity sensor was measured. In conclusion, the sensor has a high sensitivity of over 640 000% in the range of 40–100% RH, a fast response time (≈25 s), hysteresis (within 5%), and long-term stability (over 14 days). The sensor property is satisfied for the measurement of skin humidity.

Next, the influence of other factors is investigated. Because of its mechanical flexibility under pressing and bending, the sensor can be attached to human skin and perform continuous, stable long-term monitoring without adversely affecting the skin. Also, the sensor is stable under stretching, friction, objects approaching, it is able to work under different kinds of influence.

Furthermore, the impedance analysis was performed. An equivalent circuit model was built, and the impedance curve fitting based on the equivalent circuit was performed. The change trend of the resistor and capacitor components were concluded.

Finally, the application of the sensor for the continuous monitoring of skin humidity was accomplished. First, the distribution of the humidity values along the skin surface was measured. Next, one-hour continuous monitoring of skin humidity was performed. The comparison of the nanomesh humidity sensor measurement results and the commercial humidity sensor measurement results show the applicability of the nanomesh sensor.

Table 7.1 shows the comparison of the performance of the proposed sensor with the previously reported results.

Table 7.1 Comparison of performance of proposed sensor with previous reported state-of-art humidity sensors

Materials	Sensor type	RH range	Sensitivity	Sensitivity over 60%–100% (If applicable)	Gas-Permeability	Flexibility	Response/ Recovery time	Hysteresis	Reference
$Ba_{0.6}Sr_{0.4}TiO_3$–$MgTiO_3$	Resistance	5-92	5,000,000%	10,000%	No	No	/	/	[79]
KCl-doped SnO_2	Impedance	11-95	10,000,000%	400,000%	No	No	6/7 s	3%	[76]
PPPS	Impedance	9-98	10,000,000%	100,000%	No	No	1 s	5%	[44]
MoS_2 FET	Resistance	0-60	100,000,000%	/	No	Yes (1% strain)	0.1 s	/	[80]
PA66 nanofiber	Resistance	0-90	36%	28%	No	Yes (Fold, twist, knot)	/	/	[81]
Cleancool(Textile product) Yarn	Capacitance	6-97	200,000%	17,000%	No	Yes (bending)	3.5 / 4 s	/	[82]
PVA/TiC Nanofiber on substrate	Capacitance	1-90	10,000,000%	100,000%	No	No	2.8/1.7 s	2.8 %	[83]
PVA / Mxene Nanofiber on substrate	Resistance	11-97	4,000%	1,000%	No	Yes	0.9/6.3 s	1.8 %	[84]
PVA / Au	Resistance	25-97	34%	32%	Yes	Yes	148 / 110 s	/	[29]
PVA/PU nanomesh	Impedance	9-97	1,390,000%	640,000% (Best)	Yes	Yes (Pressing, Bending)	5 / 25 s	5 %	This work

7.2 prospect

In the future, first of all, the sensor's properties under the continuous attachment to the skin need to be systematically investigated. The properties such as the stability of long-term sweat immersion need to be taken into account. Also, at the same time, the influence of the stretching need to be considered. The stretchability larger than 20% strain need to be considered. One of the solutions is the utilization of the PDMS dip-coated PU nanomesh sheet.

Another important issue for application is the integration of the current sensor with other wearable sensors for a complete measurement of the skin sweating conditions. The sweat sensor that can detect the concentration of different chemicals is suitable to integrate with humidity sensor and temperature sensor together for a multimodal measurement. The integration with wearable power sources and flexible signal processing circuit and wireless module helps to realize the fully wearable system.

Reference

[1] Y. Liu, M. Pharr, and G. A. Salvatore, "Lab-on-skin: a review of flexible and stretchable electronics for wearable health monitoring," *ACS nano,* vol. 11, no. 10, pp. 9614-9635, 2017.

[2] T. Someya and M. Amagai, "Toward a new generation of smart skins," *Nat. Biotechnol.,* vol. 37, no. 4, pp. 382-388, 2019.

[3] T. R. Ray *et al.*, "Bio-Integrated Wearable Systems: A Comprehensive Review," *Chem. Rev.,* vol. 119, no. 8, pp. 5461-5533, 2019/04/24 2019, doi: 10.1021/acs.chemrev.8b00573.

[4] M. Al-Khafajiy *et al.*, "Remote health monitoring of elderly through wearable sensors," *Multimedia Tools and Applications,* vol. 78, no. 17, pp. 24681-24706, 2019.

[5] O. S. Albahri *et al.*, "Systematic review of real-time remote health monitoring system in triage and priority-based sensor technology: Taxonomy, open challenges, motivation and recommendations," *J. Med. Syst.,* vol. 42, no. 5, pp. 1-27, 2018.

[6] M. Malik *et al.*, "Electronic gadgets and their health-related claims," *Int. J. Cardiol.,* vol. 258, pp. 163-164, 2018.

[7] S. Li *et al.*, "Physical sensors for skin-inspired electronics," *InfoMat,* vol. 2, no. 1, pp. 184-211, 2020.

[8] K. Xu, Y. Lu, and K. Takei, "Multifunctional skin-inspired flexible sensor systems for wearable electronics," *Advanced Materials Technologies,* vol. 4, no. 3, p. 1800628, 2019.

[9] J. A. Rogers, T. Someya, and Y. Huang, "Materials and mechanics for stretchable electronics," *Science,* vol. 327, no. 5973, pp. 1603-7, Mar 26 2010, doi: 10.1126/science.1182383.

[10] D.-H. Kim *et al.*, "Epidermal Electronics," *Science,* vol. 333, no. 6044, pp. 838-843, 2011, doi: doi:10.1126/science.1206157.

[11] M. L. Hammock, A. Chortos, B. C. K. Tee, J. B. H. Tok, and Z. Bao, "25th

anniversary article: the evolution of electronic skin (e-skin): a brief history, design considerations, and recent progress," *Adv. Mater.,* vol. 25, no. 42, pp. 5997-6038, 2013.

[12] T. Sekitani and T. Someya, "Stretchable, large-area organic electronics," *Adv. Mater.,* vol. 22, no. 20, pp. 2228-2246, 2010.

[13] D.-H. Kim *et al.*, "Dissolvable films of silk fibroin for ultrathin conformal bio-integrated electronics," *Nature materials,* vol. 9, no. 6, pp. 511-517, 2010.

[14] S. Wang *et al.*, "Skin electronics from scalable fabrication of an intrinsically stretchable transistor array," *Nature,* vol. 555, no. 7694, pp. 83-88, 2018/03/01 2018, doi: 10.1038/nature25494.

[15] M. Shin, J. H. Song, G. H. Lim, B. Lim, J. J. Park, and U. Jeong, "Highly stretchable polymer transistors consisting entirely of stretchable device components," *Adv. Mater.,* vol. 26, no. 22, pp. 3706-3711, 2014.

[16] J. Y. Oh *et al.*, "Intrinsically stretchable and healable semiconducting polymer for organic transistors," *Nature,* vol. 539, no. 7629, pp. 411-415, 2016.

[17] H. Lee *et al.*, "Wearable/disposable sweat-based glucose monitoring device with multistage transdermal drug delivery module," *Science advances,* vol. 3, no. 3, p. e1601314, 2017.

[18] A. Miyamoto *et al.*, "Inflammation-free, gas-permeable, lightweight, stretchable on-skin electronics with nanomeshes," *Nat. Nanotechnol.,* vol. 12, no. 9, pp. 907-913, 2017.

[19] G. Korotcenkov, *Handbook of Humidity Measurement, Volume 1: Spectroscopic Methods of Humidity Measurement*. CRC Press, 2018.

[20] A. Lorek, A. Koncz, and R. Wernecke, "Development of a gas flow independent coulometric trace humidity sensor for aerospace and industry," in *Proceedings of the First European Conference on Moisture Measurement, Aquametry 2010*, 2010: MFPA Weimar, pp. 289-296.

[21] K. Xu, Y. Lu, and K. Takei, "Flexible hybrid sensor systems with feedback functions," *Adv. Funct. Mater.,* vol. 31, no. 39, p. 2007436, 2021.

[22] Y. Lu *et al.*, "Wireless and flexible skin moisture and temperature sensor sheets toward the study of thermoregulator center," *Adv. Healthc. Mater.,* vol. 10, no. 17, p. 2100103, 2021.

[23] Y. Pang *et al.*, "Wearable humidity sensor based on porous graphene network for respiration monitoring," *Biosens. Bioelectron.,* vol. 116, pp. 123-129, 2018.

[24] T. Q. Trung, L. T. Duy, S. Ramasundaram, and N.-E. Lee, "Transparent, stretchable, and rapid-response humidity sensor for body-attachable wearable electronics," *Nano Research,* vol. 10, no. 6, pp. 2021-2033, 2017.

[25] S. J. Choi *et al.*, "Nitrogen-doped single graphene fiber with platinum water dissociation catalyst for wearable humidity sensor," *Small,* vol. 14, no. 13, p. 1703934, 2018.

[26] L. Zhang *et al.*, "Wirelessly powered multi-functional wearable humidity sensor based on RGO-WS2 heterojunctions," *Sens. Actuators B Chem.,* vol. 329, p. 129077, 2021.

[27] Y. Luo, Y. Pei, X. Feng, H. Zhang, B. Lu, and L. Wang, "Silk fibroin based transparent and wearable humidity sensor for ultra-sensitive respiration monitoring," *Materials Letters,* vol. 260, p. 126945, 2020.

[28] K. Guravaiah and S. S. Raju, "e-Agriculture: Irrigation System based on Weather Forecasting," in *2020 IEEE 15th International Conference on Industrial and Information Systems (ICIIS)*, 2020: IEEE, pp. 617-622.

[29] W. Jeong, J. Song, J. Bae, K. R. Nandanapalli, and S. Lee, "Breathable nanomesh humidity sensor for real-time skin humidity monitoring," *ACS Appl. Mater. Interfaces,* vol. 11, no. 47, pp. 44758-44763, 2019.

[30] Z. Li *et al.*, "Real-time monitoring of plant stresses via chemiresistive profiling of leaf volatiles by a wearable sensor," *Matter,* vol. 4, no. 7, pp. 2553-2570, 2021.

[31] A. Kapic, A. Tsirou, P. G. Verdini, and S. Carrara, "Humidity sensors for high energy physics applications: A review," *IEEE Sens. J.,* vol. 20, no. 18, pp. 10335-10344, 2020.

[32] L. Fang, G. Clausen, and P. O. Fanger, "Impact of temperature and humidity on perception of indoor air quality during immediate and longer whole-body exposures," *Indoor Air,* vol. 8, no. 4, pp. 276-284, 1998.

[33] J. Toftum, A. S. Jørgensen, and P. O. Fanger, "Upper limits of air humidity for preventing warm respiratory discomfort," *Energy and Buildings,* vol. 28, no. 1, pp. 15-23, 1998.

[34] W. E. Bradshaw and C. M. Holzapfel, "Evolutionary response to rapid climate change," *Science,* vol. 312, no. 5779, pp. 1477-1478, 2006.

[35] T. P. Yeo, "Heat stroke: a comprehensive review," *AACN Adv. Crit. Care,* vol. 15, no. 2, pp. 280-293, 2004.

[36] K. Engebretsen, J. Johansen, S. Kezic, A. Linneberg, and J. Thyssen, "The effect of environmental humidity and temperature on skin barrier function and dermatitis," *J. Eur. Acad. Dermatol. Venereol.,* vol. 30, no. 2, pp. 223-249, 2016.

[37] M. G. Lawrence, "The relationship between relative humidity and the dewpoint temperature in moist air: A simple conversion and applications," *Bulletin of the American Meteorological Society,* vol. 86, no. 2, pp. 225-234, 2005.

[38] I. Fratoddi, A. Bearzotti, I. Venditti, C. Cametti, and M. Russo, "Role of nanostructured polymers on the improvement of electrical response-based relative humidity sensors," *Sens. Actuators B Chem.,* vol. 225, pp. 96-108, 2016.

[39] B. Yang, B. Aksak, Q. Lin, and M. Sitti, "Compliant and low-cost humidity nanosensors using nanoporous polymer membranes," *Sens. Actuators B Chem.,* vol. 114, no. 1, pp. 254-262, 2006.

[40] S. Borini *et al.*, "Ultrafast graphene oxide humidity sensors," *ACS nano,* vol. 7, no. 12, pp. 11166-11173, 2013.

[41] J. Wu *et al.*, "Carbon nanocoil-based fast-response and flexible humidity sensor for multifunctional applications," *ACS Appl. Mater. Interfaces,* vol. 11, no. 4, pp. 4242-4251, 2019.

[42] L. Ma *et al.*, "Full-Textile Wireless Flexible Humidity Sensor for Human Physiological Monitoring," *Adv. Funct. Mater.,* vol. 29, no. 43, p. 1904549,

2019.

[43] N. Li *et al.*, "High-performance humidity sensor based on urchin-like composite of Ti3C2 MXene-derived TiO2 nanowires," *ACS Appl. Mater. Interfaces,* vol. 11, no. 41, pp. 38116-38125, 2019.

[44] J. Zhou *et al.*, "Surface modification of polysquaraines to sense humidity within a second for breath monitoring," *Sens. Actuators B Chem.,* vol. 271, pp. 137-146, 2018.

[45] A. Alakanandana, A. Subrahmanyam, and J. S. Kumar, "Structural and electrical conductivity studies of pure PVA and PVA doped with succinic acid polymer electrolyte system," *Materials Today: Proceedings,* vol. 3, no. 10, pp. 3680-3688, 2016.

[46] P. Dutta, S. Biswas, M. Ghosh, S. De, and S. Chatterjee, "The dc and ac conductivity of polyaniline–polyvinyl alcohol blends," *Synthetic metals,* vol. 122, no. 2, pp. 455-461, 2001.

[47] M. Tommalieh, H. A. Ibrahium, N. S. Awwad, and A. Menazea, "Gold nanoparticles doped polyvinyl alcohol/chitosan blend via laser ablation for electrical conductivity enhancement," *Journal of Molecular Structure,* vol. 1221, p. 128814, 2020.

[48] K. Hemalatha, G. Sriprakash, M. Ambika Prasad, R. Damle, and K. Rukmani, "Temperature dependent dielectric and conductivity studies of polyvinyl alcohol-ZnO nanocomposite films by impedance spectroscopy," *Journal of Applied physics,* vol. 118, no. 15, p. 154103, 2015.

[49] N. Athanasopoulos, A. Baltopoulos, M. Matzakou, A. Vavouliotis, and V. Kostopoulos, "Electrical conductivity of polyurethane/MWCNT nanocomposite foams," *Polymer Composites,* vol. 33, no. 8, pp. 1302-1312, 2012.

[50] H. Honarkar, "Waterborne polyurethanes: A review," *Journal of Dispersion Science and Technology,* vol. 39, no. 4, pp. 507-516, 2018.

[51] X. Zhao, X. Chen, X. Yu, P. Du, N. Li, and X. Chen, "Humidity-sensitive

properties of TiO 2 nanorods grown between electrodes on Au interdigital electrode substrate," *IEEE Sens. J.,* vol. 17, no. 19, pp. 6148-6152, 2017.

[52] E. O. Doebelin and D. N. Manik, "Measurement systems: application and design," 2007.

[53] J. G. Webster, *Medical instrumentation: application and design*. John Wiley & Sons, 2009.

[54] https://en.wikipedia.org/wiki/Wetting.

[55] M. Matsuguchi, S. Umeda, Y. Sadaoka, and Y. Sakai, "Characterization of polymers for a capacitive-type humidity sensor based on water sorption behavior," *Sens. Actuators B Chem.,* vol. 49, no. 3, pp. 179-185, 1998.

[56] Y. Sakai, Y. Sadaoka, and M. Matsuguchi, "Humidity sensors based on polymer thin films," *Sens. Actuators B Chem.,* vol. 35, no. 1-3, pp. 85-90, 1996.

[57] A. Miyamoto, H. Kawasaki, S. Lee, T. Yokota, M. Amagai, and T. Someya, "Highly Precise, Continuous, Long-term Monitoring of Skin Electrical Resistance by Nanomesh Electrodes," *Adv. Healthc. Mater.,* p. 2102425, 2022.

[58] Y. Wang *et al.*, "Robust, self-adhesive, reinforced polymeric nanofilms enabling gas-permeable dry electrodes for long-term application," *Proc. Natl. Acad. Sci.,* vol. 118, no. 38, p. e2111904118, 2021.

[59] Z. Bao, Y. Feng, A. Dodabalapur, V. R. Raju, and A. J. Lovinger, "High-Performance Plastic Transistors Fabricated by Printing Techniques," *Chem. Mater.,* vol. 9, no. 6, pp. 1299-1301, 1997/06/01 1997, doi: 10.1021/cm9701163.

[60] F. Garnier, R. Hajlaoui, A. Yassar, and P. Srivastava, "All-Polymer Field-Effect Transistor Realized by Printing Techniques," *Science,* vol. 265, no. 5179, pp. 1684-1686, 1994, doi: doi:10.1126/science.265.5179.1684.

[61] E. Menard *et al.*, "Micro- and Nanopatterning Techniques for Organic Electronic and Optoelectronic Systems," *Chem. Rev.,* vol. 107, no. 4, pp. 1117-1160, 2007/04/01 2007, doi: 10.1021/cr050139y.

[62] S. R. Forrest and M. E. Thompson, "Introduction: Organic Electronics and Optoelectronics," *Chem. Rev.,* vol. 107, no. 4, pp. 923-925, 2007/04/01 2007,

doi: 10.1021/cr0501590.

[63] Y. Qiao *et al.*, "Graphene-based wearable sensors," *Nanoscale,* vol. 11, no. 41, pp. 18923-18945, 2019.

[64] Q. Cao and J. A. Rogers, "Ultrathin Films of Single-Walled Carbon Nanotubes for Electronics and Sensors: A Review of Fundamental and Applied Aspects," *Adv. Mater.,* vol. 21, no. 1, pp. 29-53, 2009.

[65] Z. Fan *et al.*, "Toward the Development of Printable Nanowire Electronics and Sensors," *Adv. Mater.,* vol. 21, no. 37, pp. 3730-3743, 2009.

[66] S. Lee *et al.*, "Nanomesh pressure sensor for monitoring finger manipulation without sensory interference," *Science,* vol. 370, no. 6519, pp. 966-970, 2020.

[67] S. Lee *et al.*, "Ultrasoft electronics to monitor dynamically pulsing cardiomyocytes," *Nat. Nanotechnol.,* vol. 14, no. 2, pp. 156-160, 2019.

[68] J. Jacquelin, "A number of models for CPA impedances of conductors and for relaxation in non-Debye dielectrics," *Journal of non-crystalline solids,* vol. 131, pp. 1080-1083, 1991.

[69] A. Jonscher, "Analysis of the alternating current properties of ionic conductors," *JMatS,* vol. 13, no. 3, pp. 553-562, 1978.

[70] C.-D. Feng, S.-L. Sun, H. Wang, C. U. Segre, and J. R. Stetter, "Humidity sensing properties of Nation and sol-gel derived SiO2/Nafion composite thin films," *Sens. Actuators B Chem.,* vol. 40, no. 2-3, pp. 217-222, 1997.

[71] J. Wang, Q. Lin, R. Zhou, and B. Xu, "Humidity sensors based on composite material of nano-BaTiO3 and polymer RMX," *Sens. Actuators B Chem.,* vol. 81, no. 2-3, pp. 248-253, 2002.

[72] K. Ogura, T. Tonosaki, and H. Shiigi, "AC impedance spectroscopy of humidity sensor using poly (o-phenylenediamine)/poly (vinyl alcohol) composite film," *J. Electrochem. Soc.,* vol. 148, no. 3, p. H21, 2001.

[73] S.-H. Song, X. Wang, and P. Xiao, "Effect of microstructural features on the electrical properties of TiO2," *Mater. Sci. Eng. B,* vol. 94, no. 1, pp. 40-47, 2002.

[74] B. Datta, *Numerical methods for linear control systems*. Academic Press, 2004.

[75] K.-S. Chou, T.-K. Lee, and F.-J. Liu, "Sensing mechanism of a porous ceramic as humidity sensor," *Sens. Actuators B Chem.,* vol. 56, no. 1-2, pp. 106-111, 1999.

[76] X. Song, Q. Qi, T. Zhang, and C. Wang, "A humidity sensor based on KCl-doped SnO2 nanofibers," *Sens. Actuators B Chem.,* vol. 138, no. 1, pp. 368-373, 2009.

[77] W. Bolton, *Instrumentation and control systems*. Newnes, 2021.

[78] T. W. Napporn *et al.*, "Electrochemical measurement methods and characterization on the cell level," in *Fuel Cells and Hydrogen*: Elsevier, 2018, pp. 175-214.

[79] S. Ke, H. Huang, H. Fan, H. Chan, and L. M. Zhou, "Structural and electric properties of barium strontium titanate based ceramic composite as a humidity sensor," *Solid State Ion.,* vol. 179, no. 27-32, pp. 1632-1635, 2008.

[80] J. Zhao *et al.*, "Skin-Inspired High-Performance Active-matrix Circuitry for Multimodal User-Interaction," *Adv. Funct. Mater.,* vol. 31, no. 38, p. 2105480, 2021.

[81] L. Lu, C. Jiang, G. Hu, J. Liu, and B. Yang, "Flexible noncontact sensing for human–machine interaction," *Adv. Mater.,* vol. 33, no. 16, p. 2100218, 2021.

[82] L. Ma *et al.*, "Full-textile wireless flexible humidity sensor for human physiological monitoring," *Adv. Funct. Mater.,* vol. 29, no. 43, p. 1904549, 2019.

[83] S. Mazhar *et al.*, "Electrospun PVA/TiC nanofibers for high performance capacitive humidity sensing," *Microchem. J.,* vol. 157, p. 104974, 2020.

[84] D. Wang, D. Zhang, P. Li, Z. Yang, Q. Mi, and L. Yu, "Electrospinning of flexible poly (vinyl alcohol)/MXene nanofiber-based humidity sensor self-powered by monolayer molybdenum diselenide piezoelectric nanogenerator," *Nano-micro letters,* vol. 13, no. 1, pp. 1-13, 2021.

Acknowledgements

First of all, I would like to express my sincere and great appreciation and respect to my supervisor, Professor Takao Someya. Professor Someya is one of the world-leading scientists in the field of flexible electronics. Under the support from him, I know how the research of a world-class should be. His rigorous attitude towards research, profound insights and accurate grasp of the research direction always infects me and guide me to persist on the road of research. I was deeply moved by his insight, passion and guide and decide to continue my PhD course study and research still under the supervision of him.

I am greatly thankful to Prof. Tomoyuki Yokota for his always patient guidance and professional instruction and help during my learning and research. His profound knowledge on the organic electronics and wearable sensors lead me into a new field that I have not experienced before. Whenever I meet any obstacles and difficulties, the help and advice from him can always guide me to the correct direction and find new achievements.

I would like to express my special thankful and appreciation to Prof. Sunghoon Lee. Prof. Lee is the specialist in the fabrication, characterization of nanomesh sensors. Without his help, I can never know the experiment skills so fast. His years of research experience made him full of experience, and his kind help makes me come through the most difficult times during the research.

I would like to express appreciation to Prof. Kenjiro Fukuda. He is specialist in organic electronics and organic solar cells. In my research life, he usually catch my problems in presentations and give me valuable comments and help. Also, during my experiments, I need to visit Riken for the equipment. His guide helped me a lot.

When I started my research work, the senior post-doctoral lab members, including Dr. Yan Wang, Dr. Chunya Wang, Dr. Binghao Wang, Dr. JaeJoon Kim, were active in both

experiments and discussion. In every consultation, discussion, and joint experiments, I gradually mastered experimental skills, learned the methods of scientific exploration, and become interested in science research life. I am very grateful to have such professional, mature and enthusiastic seniors as my model in the early stage of my research.

I especially want to thank Dr. Zhi Jiang, Dr. Jiabin Wang, Mr. Haoyang Wang, Mr. Dongkai Cheng and Ms. Jiachen Wang, the seniors who interacted with me the most in the lab. In my moments of hesitation and doubt, they stood by me steadfastly. When I knew very little about research, they were able to discuss relevant knowledge with me and solve my doubts. At the same time, life in a foreign country is difficult and full of unknowns, as fellow compatriots, they also helped me a lot on life in Japan.

The senior members in the lab, including Dr. Yusaku Tagawa, Dr. Yasutoshi Jimbo, Dr. Md Osman Goni Nayeem, Dr. Chihiro Okutani, Mr. Yu Kato, Mr. Suksmandhira Harimurti, Mr. Shuhei Shimanoe, Mr. Iwao Shirayama, Mr. Takafumi Ishigaki, Mr. Kanta Takano, Mr. Yutaro Sumi, Mr, Takuto Aiura, Mr. Yusei Nakamura, all of them are good at their own works. Every day in the lab I learn from them, exchange experiences, and discuss research progress. I am fortunate to have met so many wonderful people

I also want to thank to the Someya group Riken members, including Dr. Steven Rich, Dr. Sixing Xiong, Dr. Lulu Sun, Mr. Masahito Takakuwa, Mr. Baocai Du, Mr. Tatsuma Miyake, Mr. Shumpei Katayama, Mr. Motoshi Tanaka. They work hard in the related field and we hold discussions together in the group meeting. Their professional insights in their respective fields are invaluable role models on my learning path.

I would also like to thank fellow members in Someya lab, including Mr. Yutaro Kato, Mr. Kazuma Mori, Mr. Theodorus Wijaya, Ms. Shuyang Guo, Ms. Chika Okuda, Mr. Yusuke Ebihara, Ms. Jiaying Xu, Mr. Hiroo Miyata, Mr. Kosei Sasaki, Ms. Maho Mimuro, Ms. Tamaki Miyase, Mr. Nao Sumi. Their thinking about research problems, their enthusiasm for life, and their friendship with me all make me grow up and become

a better person.

I would also like to thank the technical staff and secretaries in Someya group, including Dr. Miyamoto, Ms. Yoko Tashiro, Mr. Yutaro Tachibana, Ms. Mari Koizumi, Ms. Wakako Yukita, Ms. Kazuyo Matsuoka, Ms. Tomoko Ikegaya, Ms. Shoko Yamazaki, Ms. Satsuki Hara. In the everyday life in laboratories, there always exist so many difficulties, without your help, I can not imagine how I can overcome these difficulties and reach the current achievements. I will never forget your assistance with my clumsy experiment skills and my poor Japanese.

Finally, I would like to express my great thankfulness and love to my parents. It is you who bring me to this world and give me all the possibilities. Thank you for your unconditional support and understanding during my life abroad in Japan.

Achievements

Published journal papers related to this work:

[1] **Wenqing Wang**, Md Osman Goni Nayeem, Haoyang Wang, Chunya Wang, JaeJoon Kim, Wang, Binghao Wang, Sunghoon Lee, Tomoyuki Yokota, Takao Someya. “Gas-permeable highly sensitive nanomesh humidity sensor for continuous measurement of skin humidity.” 2022, 2200479.

Other Published journal papers:

[1] Bin Xiang, **Wenqing Wang**, Hongxu Li, Lei Gao, Zhiyuan Liu, Yingsan Geng, Jianhua Wang, and Youping Tu. (2021) "Study on the influencing factors to reduce the recovery time of superconducting tapes and coils for the DC superconducting fault current limiter applications." High Voltage, 1-15.

Conference presentations

[1] **Wenqing Wang**, Md Osman Goni Nayeem, Haoyang Wang, Binghao Wang, Sunghoon Lee, Tomoyuki Yokota, Takao Someya, “Highly sensitive nanomesh-based humidity sensor for skin moisture detection.” FSE 2nd event, Virtual, June 2021.

[2] **Wenqing Wang**, Md Osman Goni Nayeem, Haoyang Wang, Sunghoon Lee, Tomoyuki Yokota, Takao Someya, “A flexible and gas-permeable nanomesh humidity sensor with a high sensitivity.” FSE 3rd event, Virtual, December 2021.

[3] **Wenqing Wang**, Md Osman Goni Nayeem, Haoyang Wang, Chunya Wang, Jae Joon Kim, Binghao Wang, Sunghoon Lee, Tomoyuki Yokota, Takao Someya, “A novel gas-permeable nanomesh humidity sensor with high sensitivity. ” SSDM2022, Makuhari, Chiba, Japan, September, 2022.(Accepted)

Awards

FSE Best presentation awards, Young Researchers Society for Flexible and Stretchable Electronics, 2021.